HHS Public Access

Author manuscript

Dev Biol. Author manuscript; available in PMC 2023 January 01.

Published in final edited form as:

Dev Biol. 2022 January ; 481: 75–94. doi:10.1016/j.ydbio.2021.09.007.

Asymmetric organelle positioning during epithelial polarization of *C. elegans* intestinal cells

James N. Brandt[1], **Laura Voss**[1], **Fiona M. Rambo**, **Katelyn Nicholson**, **Jackson R. Thein**, **Lydia Fairchild**, **Laurence Seabrook**, **Danielia Lewis**, **Lali Guevara-Hernandez**, **Matthew L. White**, **Luca Sax**, **Victoria Eichten**, **Logan Harper**, **Greg J. Hermann***

Department of Biology, Lewis & Clark College, Portland, OR, USA

Abstract

While the epithelial cell cortex displays profound asymmetries in protein distribution and morphology along the apico-basal axis, the extent to which the cytoplasm is similarly polarized within epithelial cells remains relatively unexplored. We show that cytoplasmic organelles within *C. elegans* embryonic intestinal cells develop extensive apico-basal polarity at the time they establish cortical asymmetry. Nuclei and conventional endosomes, including early endosomes, late endosomes, and lysosomes, become polarized apically. Lysosome-related gut granules, yolk platelets, and lipid droplets become basally enriched. Removal of *par-3* activity does not disrupt organelle positioning, indicating that cytoplasmic apico-basal asymmetry is independent of the PAR polarity pathway. Blocking the apical migration of nuclei leads to the apical positioning of gut granules and yolk platelets, whereas the asymmetric localization of conventional endosomes and lipid droplets is unaltered. This suggests that nuclear positioning organizes some, but not all, cytoplasmic asymmetries in this cell type. We show that gut granules become apically enriched when WHT-2 and WHT-7 function is disrupted, identifying a novel role for ABCG transporters in gut granule positioning during epithelial polarization. Analysis of WHT-2 and WHT-7 ATPase mutants is consistent with a WHT-2/WHT-7 heterodimer acting as a transporter in gut granule positioning. In *wht-2(−)* mutants the polarized distribution of other organelles is not altered and gut granules do not take on characteristics of conventional endosomes that could have explained their apical mispositioning. During epithelial polarization *wht-2(−)* gut granules exhibit a loss of the Rab32/38 family member GLO-1 and ectopic expression of GLO-1 is sufficient to rescue the basal positioning of *wht-2(−)* and *wht-7(−)* gut granules. Furthermore, depletion of GLO-1 causes the mislocalization of the endolysosomal RAB-7 to gut granules and RAB-7 drives the apical mispositioning of gut granules when GLO-1, WHT-2, or WHT-7 function is disrupted. We suggest that ABC transporters residing on gut granules can regulate Rab dynamics to control organelle positioning during epithelial polarization.

*Corresponding author. Department of Biology, Lewis & Clark College, Portland, OR, USA, hermann@lclark.edu (G.J. Hermann).

[1]The authors contributed equally to the work

Graphical Abstract

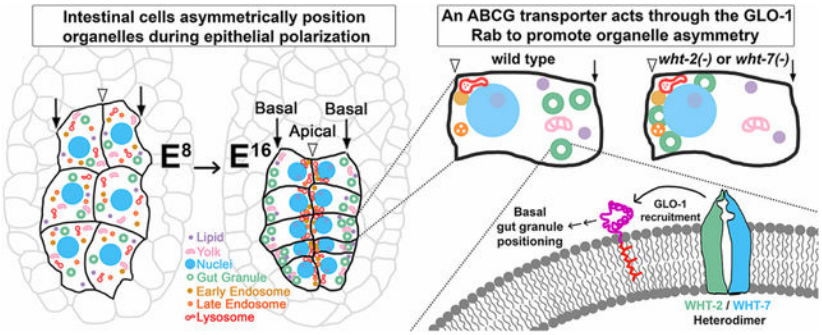

Keywords

epithelial polarization; organelle positioning; ABC transporter; Rab GTPase; *C. elegans*

Introduction

The epithelial cells lining the interior and exterior surfaces of organs and tissues function as barriers, promote selective transport, and provide mechanical strength in embryos and mature organisms [1]. Epithelial cells characteristically segregate the cell cortex, including both the plasma membrane and underlying cytoplasm, into distinct apical, lateral, and basal domains [2]. The outward facing apical domain often harbors specialized structures such as microvilli or cilia, the lateral domain contacts other epithelial cells and contains cell-cell junction complexes, and the basal domain opposes the apical domain, typically interacting with the extracellular matrix [3]. Epithelial cells can also exhibit pronounced apico-basal polarity in the distribution of their cytoplasmic organelles, resulting in important physical and functional characteristics [4, 5].

Well-studied and conserved PAR, CRB, and SCRB polarity complexes mediate the apico-basolateral polarization of the epithelial cell cortex [2, 6]. These complexes collaborate with endosomal organelles to establish and maintain the selective trafficking of proteins to the apical or basolateral plasma membrane [7–9]. The polarity complexes also influence the localization of recycling endosomes normally associated with the apical domain of epithelial cells [10]. For most epithelia, it remains an open question which organelles are asymmetrically positioned and whether the polarity complexes direct their segregation within the cytoplasm.

The polarization of intestinal epithelial cells has been extensively studied in *C. elegans* embryos [2, 11]. Midway through embryogenesis, two rows of intestinal cells rapidly polarize so that their apical surface faces a lumen positioned between the two sides of the bilaterally symmetric intestinal primordium [12]. In these cells, the cortical PAR complex protein PAR-3 is both the most upstream regulator and first protein known to be asymmetrically localized during epithelial polarization [13]. While the intestinal cell cortex is being segregated into apical and basolateral domains, nuclei and centrioles become asymmetrically localized toward the apical domain whereas lysosome related organelles

(LROs) called gut granules become basally enriched [12–15], suggesting that the cytoplasm becomes polarized during this time as well. At the end of embryogenesis, recycling endosomes, early endosomes, late endosomes, and lysosomes are enriched near the apical cortex [15–17]. In adults, recycling and early endosomes remain apically localized, whereas late endosomes and lysosomes are equally distributed along the apico-basal axis [10, 18, 19]. It is currently not known whether the asymmetrical positioning of endosomal compartments is coordinated with epithelial polarization during embryogenesis.

Factors functioning in endosome biogenesis can also direct the intracellular movement and localization of endosomes [20, 21]. For example, Rab5 labeled early endosomes are transformed into late endosomes marked by Rab7, which directs the removal of specific cargo and their fusion with Arf labeled lysosomes [22–25]. The same Rab and Arf GTPases that function in these endosomal protein trafficking events also mediate endosome, lysosome, and LRO motility by interacting with different sets of effectors [20, 21, 26]. Whether other components of the endosomal protein trafficking machinery mediate endosomal positioning within cells has remained relatively unexplored.

In this work we describe the apico-basal polarization of a diverse collection of organelles during the polarization of C. *elegans* intestinal epithelial cells. We show that the cytoplasmic polarization of epithelial cells does not require PAR-3 and demonstrate that apically directed nuclear migration contributes to the asymmetric distribution of some but not all basal organelles. We identify the WHT-2 and WHT-7 ABCG transporters as a key factor required for the basal localization of LROs and we show that they likely impact LRO positioning through Rab activity [27].

Materials and Methods

Mutations and strains

C. elegans strains were grown at 22°C on NGM media seeded with OP50 *Escherichia coli* [28]. N2 was used as the wild-type strain and was the background used to create the following mutations that were used in this study: *apt-6(ok429)*, *glo-2(tm592)*, *glo-3(kx38)*, *par-3(tm2716)*, *rab-7(ok511)*, *unc-83(ku18)*, *vps-18(tm1125)*, *wht-1(tm688)*, *wht-2(ok2775)*, *wht-2(gk891224)*, *wht-3(ok927)*, *wht-4(ok1007)*, *wht-5(ok806)*, *wht-6(ok882)*, *wht-7(ok812)*, *wht-7(gk692424)*, *wht-8(ok3112)*. Descriptions of each mutant allele can be found at Wormbase (www.wormbase.org). The following CRISPR genome edited alleles were used: *glo-1(syb1102[gfp::glo-1])* [27], *wht-2(syb668[K74M])* [27], *wht-2(syb745[K74R])* [27], *wht-7(syb1988[K105M])* (this work), *wht-7(syb1982[K105R])* (this work). The following transgenes were used: *amIs4[cdf-2p::cdf-2::gfp::; unc-119(+)]* [29], *hjIs67[atgl-1p::atgl-1::gfp; mec-7::rfp]* [30], *kxEx9[glo-1p::gfp::glo-1(+); Rol-6^{D}]* [15], *kxEx152[asm-1p::asm-1::mCherry; Rol-6D]* [31], *kxEx230[glo-1p::gfp::glo-1(Q71L); Rol-6^{D}]* [32], *kxEx231[glo-1::gfp::glo-1(T25N); Rol-6D]* [32], *kxEx287[wht-2p::wht-2(+); Rol-6^{D}]* [27], *kxEx288[WRM0639dG05; Rol-6^{D}]* (this work), *kxIs5[glo-1p::mans::mCherry; unc-119(+)]* [27], *ltSi910[elt-2p::vhhGFP4::zif-1::operon-linker::mCherry::his-11::tbb-2; unc-119(+)]* [33], *opIs222[eft-3p::gfp::fyve::fyve; unc-119(+)]* [34], *pwIs20[pie-1p::gfp::rab-5; unc-119(+)]*

[35], *pwIs50[lmp-1p::lmp-1::gfp; unc-119(+)]* [36], *qxIs354[ced-1p::laat-1::gfp]* [37], *tdEx2[arl-8p::arl-8::gfp; Rol-6^{D}]*[38], *zuIs20[par-3p::par-3::zf1::gfp; unc-119(+)]* [39].

Genetic manipulations

wht-2(gk891224) was identified in a screen of Million Mutation strains for mispositioning of autofluorescent gut granules in E16 stage embryos. *wht-2(ok2775)* embryos showed the same defect in gut granule positioning, which was rescued by the presence of *kxEx287[wht-2(+)]*. Both *wht-7(ok812) and wht-7(gk692424)* showed a similar defect in positioning of autofluorescent gut granules in E16 stage embryos. Gut granule positioning was restored in *wht-7(ok812)* embryos when the *wht-7(+)* containing fosmid WRM0639dG05 was injected at 5ng/μl with pRF4 at 100ng/μl. The resulting *kxEx288* array was used to score rescue.

CRISPR-Cas9-mediated gene editing was carried out by SunyBiotech (Fuzhou, Fujian, China) to generate PHX1976 *wht-2(syb1976)* and PHX1988 *wht-7(syb1988)*, which precisely change lysine 105 to methionine, and PHX1982 *wht-7(syb1982)* and PHX2008 *wht-7(syb2008)*, which precisely change lysine 105 to arginine. The mutations were verified with Sanger DNA sequencing. The sequence of the first 65 nucleotides of exon four of the *wht-7* K105M and K105R mutations are shown:

K105M—

TGTTCGGAGTGGCTCGACCCGGAGAGGTTACgGCGATCATTGGgCCCAGTGGAGC
TGGcATGACT

K105R—

TGTTCGGAGTGGCTCGACCCGGAGAGGTTACgGCGATCATTGGgCCCAGTGGAGC
TGGgCGCACT

The underlined upper case nucleotides indicate the point mutations changing K105 and the underlined lower case nucleotides indicate the synonymous mutations that alter the sgRNA or protospacer adjacent motif to prevent recutting by CRISPR-Cas9. The positioning of gut granules was normal in the K105M and K105R alleles; *wht-7(syb1988[K105M])* and *wht-7(syb1982[K105R])* were used in this study.

wht-2(K74M/R); wht-7(K105M/R) double mutants were generated using *wht-2(K74M/R); wht-7(ok812)* deletion strains. These strains were created by mating *wht-7(ok812)* males with *wht-2(K74M/R)* point mutants and isolating resulting lines that mislocalized autofluorescent gut granules apically in E16 stage embryos, indicating that *wht-7(ok812)* was homozygous, and that lacked birefringent gut granules at the 1.5-fold stage embryos, indicating that *wht-2(K74M/R)* was present. The presence of the *wht-2* point mutation and *wht-7* deletion in these strains was verified by Sanger DNA sequencing (Genewiz, South Plainfield, NJ) and PCR, respectively. *wht-2(K74M/R); wht-7(ok812)* strains were then mated with *wht-2(+); wht-7(K105M/R)* males and progeny were isolated that lacked birefringent granules in 1.5-fold stage embryos, indicating that *wht-2(K74M/R)* was homozygous, and that lacked the *wht-7(ok812)* deletion scored with PCR, indicating

wht-7(K105M/R) was homozygous. The presence of the *wht-2* and *wht-7* point mutations in the resulting strains were verified by DNA sequencing.

Transgenes were typically moved into mutant backgrounds by crossing males carrying the mutation with hermaphrodites containing the transgene. Resulting strains were confirmed to contain the extrachromosomal array, be homozygous for the mutation, or be homozygous for the integrated transgene through phenotypic analysis. The *wht-2(−); unc-83(ku18)* double mutant was identified in progeny of a cross between the single mutants that displayed both the reduction of birefringent granules in pretzel stage embryos, which indicates homozygosity for *wht-2(−)* [27], and the lack of nuclear polarization in bean stage embryonic intestinal cells, which indicates homozygosity for *unc-83(ku18)* [14]. The *wht-2(ok2775)* and *wht-7(ok812)* double mutants with *glo-3(kx38)* were identified by isolating progeny of a cross between the single mutants that displayed reduced numbers of enlarged birefringent gut granules in pretzel stage embryos, which indicates homozygosity for *glo-3(kx38)* [32], and that were also homozygous for the *wht* deletion shown by PCR screening. The *wht-2(ok2775); wht-7(ok812)* double mutant was isolated in progeny of a cross between the single mutants that showed a reduction in birefringent gut granules, which indicates homozygosity for *wht-2(ok1775)* [27], that were also homozygous for the *wht-7(ok812)* deletion shown by PCR screening. The *ltSi910[intDEG]*; *glo-1(syb1102[gfp::glo-1])* double mutant was created by crossing *glo-1(syb1102[gfp::glo-1])* with *ltSi910[intDEG]* and identifying a line that was homozygous for *glo-1(syb1102[gfp::glo-1])* and heterozygous for *ltSi910[intDEG*], which was shown by its E16 stage progeny always exhibiting GFP::GLO-1 expression except in embryos that expressed mCherry::HIS-11 from *intDEG* [33].

par-3(MZ) embryos, which lack zygotic and maternally contributed *par-3* at the E16 stage, were generated using the strategy described in [13]. *par-3(tm2716) unc-32(e189)/qC1[dpy-19(e1259); him-8(e1489)* males were mated with *par-3(tm2716) unc-32(e189); zuIs20[par-3p::par-3::zf1::gfp; unc-119(+)]* hermaphrodites. Typically 40 outcross Unc progeny, which are *par-3(tm2716) unc-32(e189)/par-3(tm2716) unc-32(e189); par-3::zf1::gfp/+*, were placed on a plate and allowed to self fertilize. The resulting embryos, ¼ of which are *par-3(MZ)*, were analyzed. *par-3(MZ)* embryos were identified in the population by the lack of PAR-3::GFP expression in the intestinal and pharynx primordia.

To target the expression of *rab-7* with RNA interference (RNAi) we used feeding protocol 1 described in [40]. The effects of *rab-7(RNAi)* were not seen in embryos exposed to inert/F33E2.4 9 (RNAi), which targets a gene not involved in gut granule biogenesis or positioning. Ahringer library clones were used for RNAi (Source Bioscience, Nottingham, UK). In RNAi experiments, inhibition of *rab-7* function was assessed by the appearance of numerous refractile bodies in embryos visualized with DIC microscopy.

Microscopy

All of the fixed and stained embryos were imaged with a Zeiss LSM710 confocal microscope using a 63x Plan-Apochromat 1.4 NA objective. Living embryos were imaged with a 100x Plan-Acrochromat 100X 1.4 NA objective using a Zeiss AxioImager.M2 widefield microscope equipped with DIC, polarization, and fluorescence optics. Images

were captured using an AxioCam MRm digital camera controlled by AxioVision 4.8 software (Zeiss, Thornwood, NY).

Living embryos were placed on a 3% agarose pad in a drop of H_2O. Polarization optics were used to visualize birefringent material in 1.5-fold and pretzel stage embryos. Autofluorescence was imaged in E16 stage embryos using a Zeiss 49 filter (DAPI, excitation G 365, emission, BP445/50). Embryos were freeze-cracked and fixed in −20°C methanol for 15 minutes [12]. In some cases the intrinsic fluorescence of GFP was used to visualize GFP tagged proteins. Antibodies to BGS-1 [41], GFP, including clones 7.1/13.1 (Sigma Aldrich) and ab6556 (abcam), IFA, which binds to centrioles and labels centrosomes [12], LMP-1, which labels lysosomes and gut granules [42], clone F-11, which binds ICL-1 labeling mitochondria [43], clone P4A1, which labels PAR-3 [39], PGP-2, which labels gut granules [44], RAB-5, which labels early endosomes [45], RAB-7, which labels late endosomes [18], and WHT-2, which labels gut granules, [27] were used. We also used two previously un-described mouse monoclonal antibodies that were identified in a screen for antibodies that label *C. elegans* embryos [46]. F2-P1C5-A5/Lateral binds only to the lateral domain of polarized epithelial cells in the intestine, pharynx, and hypodermis of *C. elegans* embryos. F2-P3E3-C3/Yolk binds to the exterior of yolk platelets in *C. elegans* embryos. The final antibody washes typically included 0.1μg/ml DAPI to stain nuclei. Z-stacks spanning the intestine of fluorescently labeled embryos were acquired with confocal microscopy.

Organelle positioning was scored in mid to late E16 stage embryos, which were defined by the developmental stage of the dorsal hypodermis. The mid E16 stage begins when hypodermal cells first extend processes to the opposing end of the contralateral cells. The late E16 stage was defined as the stage when the dorsal hypodermis was fully intercalated prior to elongation of the embryo [47]. To enable the best resolution along the apical-basal axis, only embryos that were oriented dorsal or ventral side-up were scored. Z-stacks of antibody stained embryos were analyzed for the focal plane that included the most nuclei from the dorsal tier of E16 stage intestinal cells [12]. In this optical section, the apical and basal surface of each intestinal cell (typically 10–12 were visible on the chosen focal plane) were identified by labeling the intestinal cell cortex with BGS-1 or the lateral membrane with the Lateral mAb. Occasionally, DAPI stained nuclei were used to define the apical domain as the region between contralateral intestinal nuclei and the basal domain as the surface of the underlying muscle cell nuclei. The apical to basal axis was then divided into 4 equal quadrants using a clear acetate sheet placed over the image projected on a computer monitor. The number of organelles present in each quadrant was then quantified for each intestinal cell per embryo in at least 5 different embryos. To present the data graphically, the square root of the total proportion of organelles located in each quadrant was calculated and used as the radius of the circles drawn to represent each proportion using R (version 3.1.2). Therefore, the area of each circle is directly proportional to the percentage of compartments found in that quadrant. Widefield fluorescence microscopy was used to score gut granule positioning in living embryos. After determining the correct stage and orientation with DIC microscopy, the focal plane that included the most nuclei from the dorsal tier of E16 stage intestinal cells was chosen. At this focal plane the overall pattern of autofluorescent organelles was then scored.

The SQUASSH module within FIJI was used to quantify the colocalization of fluorescent markers [48, 49]. This software segments and identifies labeled organelles within Z-stacks spanning the intestine and calculates the fraction of the volume of one marker that overlaps with the second marker.

One-way ANOVAs and Tukey-Kramer *post hoc* tests were carried out with Microsoft Excel for Mac 2011. Fisher's exact tests were carried out at www.physics.csbsju.edu/stats/exact_NROW_NCOLUMN_form.html. Dot plots were created with R. Photoshop CS2 was used to construct figures and adjustments in brightness and contrast were uniformly applied to each panel. Representative images of organelle position and marker colocalization are shown.

Data availability—Strains and antibodies are available upon request. All of the data necessary for judging the conclusions of the article are present with the figures and graphs.

Results

Asymmetric localization of organelles during epithelial polarization

Intestinal organogenesis initiates through the rapid divisions of the intestinal precursor E and its descendants, which clonally produce the twenty cells that compose the intestine [50]. The number of E descendants present within the intestinal primordium is commonly used to describe the different stages of intestinal development. Following the E8 to E16 cell divisions, E16 intestinal cells rapidly establish cell-cell junctions and cortically polarize so that their apical surface faces the intestinal lumen located at the midline between the cells on left and right sides of the bilaterally symmetric intestine [12]. The opposing basal surfaces face surrounding muscle and epidermal cells [12]. At the same time, nuclei and their associated centrosomes become asymmetrically positioned near the apical membrane [14] (Fig. 1A–B), indicating that the cytoplasm also becomes polarized at this stage of intestinal development.

To investigate whether other organelles become asymmetrically positioned in intestinal cells at the time that they establish cortical polarity, we surveyed the subcellular distribution of organelles using well-characterized organelle markers in fixed E16 stage intestinal cells. The apical and basal surfaces were identified by staining with antibodies to the β-spectrin cell cortex protein (BGS-1), by staining with a monoclonal antibody that recognizes an unidentified epitope in the lateral domain of epithelial cells (Lateral), or by labeling nuclei to aid in inferring the position of the intestinal cell cortex. We scored organelle position by subdividing intestinal cells into four equally sized quadrants along the apico-basal axis and quantified the number of organelles within each quadrant. For nuclei, which are larger than a single quadrant, we divided the apico-basal axis into thirds. The results are represented by circles that are directly proportional to the percentage of an organelle found within each quadrant (Fig 1B). Notably, most of the organelles we examined exhibited some level of asymmetry. All of the conventional endosomal organelles, including early endosomes, late endosomes, and lysosomes, were highly enriched near the apical cell membrane (Fig 1A–B). We confirmed prior work suggested that gut granules, lysosome-related organelles that are part of the endosomal system, are positioned basally (Fig 1A–B) [12, 15, 29, 51]. Yolk

platelets, lipid droplets, and to a lesser extent mitochondria, were also basally localized (Fig 1A–B). The Golgi exhibited little if any polarization along the apico-basal axis (Fig 1A–B).

To determine when these organelles become asymmetrically positioned, we analyzed their distribution along the midline to basal cell axis in the E8 stage intestinal primordium. None of the organelles we examined in E8 stage intestinal cells, including nuclei, conventional endosomes, gut granules, yolk platelets, and lipid droplets exhibited the level of polarization seen in E16 cells, often being distributed uniformly throughout the cytoplasm (Fig 2A–B). Therefore, during the E16 stage the intestinal cell cytoplasm undergoes a dramatic reorganization and polarization at the same time that intestinal cells establish cortical asymmetry along the apical-basal axis.

Nuclear polarization promotes the basal positioning of some organelles

We addressed the possibility that the localization of nuclei, which take up a significant fraction of the apical cell domain (Fig 1A), contribute to the organelle asymmetries exhibited by E16 stage intestinal cells. For example, organelles might be displaced basally in response to apical nuclear positioning or, alternatively, organelles might associate with nuclei to become apically polarized. Nuclear migration from a central position in E8 cells to the apical domain in E16 intestinal requires UNC-83 [14], which is part of the evolutionarily conserved LINC complex that mediates nuclear movements [52]. As expected for an organelle closely associated with the nucleus [53], centrosomes became displaced from the apical surface in *unc-83(ku18)* mutants that have centrally positioned nuclei (Fig 1A–B). The distribution of early endosomes, late endosomes, and lysosomes remained apical in *unc-83(−)*, showing that their asymmetric localization is independent of nuclear migration. In contrast, most of the basally polarized organelles, including gut granules and yolk platelets, became uniformly distributed along the apical-basal axis when nuclear migration was disrupted (Fig. 1A–B). Therefore, the basal polarization of some organelles might be due to their exclusion from the apical domain by the nucleus. The exceptions to this were lipid droplets, which remained basally polarized in *unc-83(−)* mutants (Fig 1A–B).

PAR-3 is dispensable for organelle asymmetry in intestinal epithelial cells

The PAR polarity proteins are central regulators of cell cortex asymmetry [54]. Notably, the PAR system mediates the asymmetric positioning of nuclear DNA and early endosomes in the one-cell *C. elegans* embryo and endosomes in adult *C. elegans* intestinal cells [10, 55, 56]. Given the requirement for PAR-3 in this process, we investigated whether PAR-3 functioned in the polarized distribution of organelles in the E16 stage intestinal primordium. We analyzed organelle positioning in *par-3(−)* embryos in which maternally supplied PAR-3 was depleted using the *par-3(MZ)* targeted protein degradation system, which has been shown to potently remove PAR-3 in E16 stage intestinal cells [13]. Early endosomes, late endosomes, and nuclei continued to be positioned apically and gut granules remained basally positioned in embryos lacking PAR-3 (Fig 3A–B), indicating that cytoplasmic polarization is independent of the PAR polarity pathway.

wht-2(−) mutants mislocalize gut granules apically

In a screen of the *C. elegans* Million Mutation collection for strains exhibiting altered LRO number or size, we identified one strain, VC40939, which mispositioned autofluorescent gut granules apically in E16 stage embryos. Each of the Million Mutation strains has had its genome sequenced and VC40939 contains *wht-2(gk891224)*, a non-sense mutation (Q49stop) that likely disrupts the function of WHT-2[57]. *wht-2* encodes an ABCG protein homologous to *Drosophila* White and mammalian ABCG proteins that promote multidrug resistance [58, 59]. We have recently shown that WHT-2 plays a role in gut granule biogenesis and localizes to E20 stage gut granules [27]. We examined WHT-2 localization in earlier embryonic stages and found that it is localized to gut granules prior to and during the stage that they become asymmetrically positioned along the apico-basal axis (Fig S1). Embryos with the *wht-2(ok2775)* null mutation showed apical gut granule mispositioning similar to *wht-2(gk891224)*, which was rescued by the addition of *wht-2(+)* (Fig 4A–B). Together these results indicate that WHT-2 functions to prevent the apical localization of gut granules.

Gut granules were often closely associated with apically localized nuclei in *wht-2(−)* mutants (Fig 4A). To determine whether gut granules become mispositioned in *wht-2(−)* mutants due to an inappropriate interaction with nuclei, we analyzed gut granule localization when nuclei were centrally positioned in *unc-83(−)*. We found that the apical localization of gut granules in *wht-2(−)* remained unchanged by the loss of *unc-83(+)* (Fig 4A–B), indicating that other processes are directing their apical accumulation.

We investigated whether the mislocalization of gut granules in *wht-2(−)* mutants results from larger changes in the apico-basal cytoplasmic polarity of E16 stage intestinal cells. As in wild type, early endosomes, late endosomes, lysosomes, nuclei, and centrosomes were apically localized in *wht-2(−)* mutants (Fig 5A–B). Similarly, the positioning of basally enriched organelles including the Golgi, yolk platelets, mitochondria, and lipid droplets were unchanged in *wht-2(−)* mutants (Fig 5A–B). These results show that cytoplasmic polarity is normal when WHT-2 function is disrupted and that the effects of *wht-2(−)* are specific to gut granule positioning.

Apical gut granules in *wht-2(−)* mutants do not resemble endolysosomes

CDF-2::GFP, which associates with gut granules in wild type [29, 51], marks apically positioned organelles in *wht-2(−)* mutants (Fig 4A–B). We found that two gut granule membrane proteins, PGP-2 and LMP-1 [44, 51], co-localized with CDF-2::GFP in E16 stage *wht-2(−)* embryos, just as they did in wild type (6A-B), making it unlikely that CDF-2::GFP is lacking from gut granules and mislocalized to apical organelles in *wht-2(−)*. In addition, *wht-2(−)* did not cause CDF-2::GFP or PGP-2 to colocalize with the lysosomal proteins ASM-1::mCherry or LAAT-1::GFP [31, 37] (Fig 6A–C), which are localized to apically positioned conventional endosomes in E16 intestinal cells (Fig 1A–B). We therefore conclude that bona fide gut granules, which are distinct from conventional lysosomes, are being apically mispositioned in *wht-2(−)* (Fig 6A–B).

LROs are part of the endolysosomal system, sharing similarities with and utilizing many of the same factors that mediate the movement of proteins between conventional endosomes [60]. We therefore addressed the possibility that gut granules in *wht-2(−)* E16 stage intestinal cells take on a conventional endosomal identity or misaccumulate endosomal positioning factors. The small GTPases RAB-5, RAB-7, and ARL-8::GFP are enriched on and can direct the movement of early endosomes, late endosomes, and lysosomes, respectively [61]. RAB-7 and ARL-8::GFP were not detectable on gut granules in wild type or *wht-2(−)* (Fig 6A–C). While we observed a slight increase in the colocalization of RAB-5 with CDF-2::GFP, *wht-2(−)* did not lead to the accumulation of early endosomal phosphatidylinositol 3-phosphate, which is bound by FYVE::GFP [62], on PGP-2 labeled gut granules (Fig 6A–C). Together, these results indicate that conventional endosomes and gut granules remain distinct when *wht-2(+)* activity is disrupted and that factors directing conventional endosome motility are not obviously mislocalized to gut granules in *wht-2(−)* mutants.

Defects in gut granule biogenesis disrupt gut granule positioning differently than *wht-2(−)*

The specific and acute mislocalization of gut granules in *wht-2(−)* suggests that in wild type, gut granules are actively prevented from localizing apically. To further explore the mechanisms governing gut granule positioning, we investigated whether gut granule identity is necessary for their basal positioning. *apt-6*, *glo-2, glo-3, rab-7*, and *vps-18* mutants disrupt protein delivery pathways leading to gut granules and have altered gut granules marked by PGP-2 [32, 51, 63]. We found that the absence of RAB-7 or the AP-3 complex subunit APT-6 had little effect on the basal positioning of gut granules (Fig 7A–B). In contrast, there was a significant increase in the proportion of gut granules localized apically when the function of the BLOC-1 subunit GLO-2, the HOPS subunit VPS-18, or the likely Rab guanine exchange factor subunit GLO-3 were disrupted (Fig 7A–B). *glo-2(tm592)* is cold sensitive for defects in gut granule biogenesis [51], and consistent with this causing gut granule mispositioning, the proportion of apical gut granules was enhanced at 15C (Fig 7A–B). Nuclei were always positioned apically in the gut granule biogenesis mutants (n= 5–26 embryos per strain).

While mutants disrupting gut granule biogenesis sometimes altered gut granule positioning, none of them led to the high levels of apical gut granule enrichment seen in *wht-2(−)* mutants. To explore whether WHT-2 promotes gut granule positioning through a role in gut granule biogenesis or through a different mechanism, we combined *wht-2(−)* with *glo-3(kx38)* and *rab-7(RNAi)*, both of which disrupt protein trafficking to gut granules [32, 63]. The addition of *glo-3(kx38)* disrupted the apical localization of gut granules caused by *wht-2(−)* and *wht-2(ok2775); glo-3(kx38)* double mutants closely resembled the *glo-3(kx38)* single mutant, where the majority of gut granules are located in basal quadrants (Fig 7A–B). *rab-7(RNAi)* similarly caused most gut granules to become basally positioned in *wht-2(−)* (Fig 7A–B). The effects of *glo-3(kx38)* and *rab-7(RNAi)* on the localization of gut granules in *wht-2(−)* suggests that gut granule identity is necessary for their apical mispositioning and that general defects in gut granule protein trafficking are unlikely to underlie the mislocalization of gut granules in *wht-2(−)*.

The ABCG protein WHT-7 functions in gut granule positioning

WHT-2 is one of eight WHT/ABCG family members in *C. elegans* [59]. ABCG proteins are often described as half transporters, due to the requirement that they homo- or heterodimerize with another ABCG protein to constitute a functional transporter [64]. To investigate whether WHT-2 functions with another ABCG protein, we analyzed autofluorescent gut granule positioning in E16 stage intestinal cells in embryos containing mutations that disrupt the function of each of the seven other *wht* genes. We found that strains containing the deletion allele *ok812* or the *gk692424* nonsense mutation, both of which are predicted to be null for *wht-7* activity, showed apical enrichment of autofluorescent organelles (Fig 8A–B). None of the other *wht* gene mutants disrupted gut granule positioning (Fig 8A–B). Introduction of a fosmid containing *wht-7(+)* into the *wht-7(ok812)* mutant restored the basal positioning of PGP-2 marked compartments (Fig 8B). The apical organelles in *wht-7(−)* appear to be properly formed gut granules based on the high level of colocalization between PGP-2 and both CDF-2::GFP and LMP-1 (Fig 9F–I). These results indicate that *wht-7(−)*, like *wht-2(−)*, causes the apical enrichment of gut granules in E16 intestinal cells.

Since both *wht-2* and *wht-7* encode ABCG proteins that could work together, we investigated the functional relationship between WHT-2 and WHT-7. Consistent with WHT-2 and WHT-7 acting in the same process, gut granule positioning in E16 intestinal cells was indistinguishable between *wht-2(−)*, *wht-7(−),* and *wht-2(−); wht-7(−)* double mutants (Fig. 9A–B). Additionally, *rab-7(RNAi)* suppressed apical gut granule mispositioning in *wht-7(−)* mutants, similar to its suppression of *wht-2(−)* (Fig. 7A–B). WHT-2 remained associated with gut granules in the *wht-7(−)* mutant at the time when gut granules polarize in E16 intestinal cells (Fig 9D–E), indicating that WHT-7 does not direct the localization of WHT-2.

In addition to functioning in gut granule positioning, WHT-2 plays a role in granule biogenesis [27]. However, unlike *wht-2(−)*, the accumulation of birefringent material within gut granules was unchanged in *wht-7(−)* and the number of birefringent gut granules in *wht-2(−); wht-7(−)* double mutants resembled the *wht-2(−)* single mutant (Fig 9C). *wht-2(−)* suppresses gut granule enlargement and enhances the loss of LMP-1 from gut granules in *glo-3(−)* mutants [27]. *wht-7(−)* mutants did not alter either of these *glo-3(−)* phenotypes (Fig S2). Additionally, *wht-2(−); wht-7(−)* double mutants did not show any reduction in the colocalization of the gut granule proteins PGP-2 and LMP-1 (Fig 9H–I). These data are consistent with WHT-2 and WHT-7 functioning similarly in gut granule positioning and highlight their different requirements for supporting gut granule biogenesis. Furthermore, they suggest that the mislocalization of gut granules in *wht-2(−)* and *wht-7(−)* is not the result of defective gut granule biogenesis.

WHT-2 and WHT-7 ATPase activity promotes gut granule positioning

The similar effects of *wht-2(−)* and *wht-7(−)* on gut granule distribution suggest that WHT-2 and WHT-7 proteins might associate and function together as a membrane transporter. We analyzed gut granule positioning in WHT-2 and WHT-7 point mutants predicted to inhibit their ATPase activity, which is essential for ABCG proteins to translocate substrates

across membranes [65]. Changing the conserved lysine in the Walker A motif to a methionine or arginine disrupts both the ATPase and transporter activity of ABCG proteins [66–68]. We have previously shown that the WHT-2(K74M) and WHT-2(K74R) point mutants partially disrupt the function of WHT-2 in gut granule biogenesis [27]. We used CRISPR/Cas9 genome editing to precisely alter the endogenous *wht-7* locus and generated WHT-7(K107M) and WHT-7(K105R) Walker A motif point mutants. The WHT-2(K74M) and both WHT-7 ATPase mutants did not disrupt gut granule positioning (Fig 10A–B). Only WHT-2(K74R) showed a discernable increase in the proportion of gut granules located in the apical domain (Fig 10A–B), however the effect was quite weak when compared to the *wht-2(−)* null mutant (Fig 4A–B).

ABCG transporters create two ATP binding sites using structural components from each of the opposing subunits [69]. If WHT-2 and WHT-7 function as homodimers, then the single ATPase mutants should disrupt their ATPase and coupled membrane transport activity. However, ABCG proteins can form heterodimers [70, 71]. If WHT-2 and WHT-7 heterodimerize, then a single functional ATPase domain would remain when a single WHT-2 or WHT-7 Walker A mutant is expressed, which can be sufficient for ABC transporter function [68, 72–74]. We therefore analyzed gut granule positioning in WHT-2 and WHT-7 ATPase double mutants and found an apical enrichment of gut granules in WHT-2(K74R); WHT-7(K105R) double mutants that approached the effect seen in *wht-2(−)* and *wht-7(−)* null mutants (Figs 4A–B, 9A–B, and 10A–B). Combining WHT-2(K74M) with either WHT-7 ATPase mutant led to a modest defect in gut granule polarization that was not seen in the single mutants (Fig 10A–B). These synergistic and synthetic genetic interactions between WHT-2 and WHT-7 ATPase mutants suggest that a WHT-2/WHT-7 heterodimer functions as a membrane transporter to promote gut granule positioning. However, none of the single or double ATPase mutants led to the strong apical enrichment seen in *wht-2(−)* or *wht-7(−)*, which could be explained by ATPase independent activity or homodimerization of WHT-2 and WHT-7 promoting basal gut granule localization.

Effects of *wht-2(−)* and *wht-7(−)* on GLO-1 Rab localization

Small GTPases, including Rabs and Arfs, localize to endosomes and mediate their intracellular localization [20, 21]. WHT-2 is necessary for the association of the Rab32/38 family member GLO-1 with E20 stage gut granules [27], an embryonic stage after gut granules become asymmetrically localized. We examined GFP::GLO-1 localization in earlier E8 and E16 stage embryos and found that GLO-1 was associated with gut granules where it could function to position gut granules in polarizing intestinal cells (Fig 11A–C). In *wht-2(−)* mutants, GFP::GLO-1 was enriched on E8 stage gut granules, however GFP::GLO-1 was lacking from gut granules in E16 stage intestinal cells (Fig 11A–C).

Given the possibility that WHT-7 functions with WHT-2 to promote gut granule positioning, we investigated the localization of GFP::GLO-1 in embryos lacking *wht-7* activity. Similar to *wht-2(−)* mutants, gut granules in E8 stage *wht-7(−)* mutants were marked by GFP::GLO-1 (Fig 11A and C). However, GFP::GLO-1 remained associated with gut granules in E16 stage *wht-7(−)* mutants (Fig 11B–C), which was surprising given evidence for the WHT-2/WHT-7 heterodimer (Fig 10). *wht-2(−); wht-7(−)* double mutants retained

GFP::GLO-1 on gut granules at the E8 stage and lacked GFP::GLO-1 on gut granules at the E16 stage, similar to *wht-2(−)* single mutants. Therefore, in contrast to WHT-2, WHT-7 is not necessary for the accumulation of GLO-1 on gut granules at the time that they are basally positioned.

GLO-1 Rab activity impacts gut granule positioning

If the loss of GLO-1 from gut granules in *wht-2(−)* leads to their apical accumulation, then the ectopic overexpression of GFP::GLO-1 might restore their basal localization. We introduced GFP::GLO-1 on an extrachromosomal array into *wht-2(−)* and found that it potently suppressed gut granule mispositioning (Fig 12A–B). To determine whether the GTPase activity of GLO-1 was necessary for this effect, we expressed GFP::GLO-1(Q71L) and GFP::GLO-1(T25N), which are predicted to be locked in the GTP and GDP-bound states, respectively. While GLO-1(Q71L) suppressed gut granule mispositioning in *wht-2(−)*, GLO-1(T25N) did not (Fig 12A–B). The expression of GLO-1(+) and GLO-1(Q71L), but not GLO-1(T25N), similarly promoted the basal localization of gut granules in *wht-7(−)* mutants (Fig 12A–B). These results are consistent with GLO-1 acting as a GTPase downstream of WHT-2 and WHT-7 to promote proper gut granule distribution.

If GLO-1 directs the basal positioning of gut granules, then disrupting its activity should alter gut granule distribution. However, *glo-1(+)* is necessary for the creation of gut granules [15, 32]. To circumvent this limitation, we targeted GLO-1 for destruction after gut granules have been created with an approach that temporally and spatially controls protein degradation [33]. In this system the intestine specific *elt-2* promoter drives the expression of a GFP nanobody::ZIF-1 fusion (called intDEG) at the E8 stage leading to potent and selective proteosomal degradation of GFP tagged proteins [33]. Combining endogenously tagged *gfp::glo-1* with intDEG led to the loss of GFP::GLO-1 from E16 intestinal cells (Fig 13A–B). In contrast to *glo-1(−)* mutants that lack gut granules [15, 32], organelles containing gut granule associated PGP-2, autofluorescent material, and WHT-2 were detected in *intDEG; gfp::glo-1* E16 intestinal cells, indicating that gut granules are present (Figs 13A, 13C, and S3). In embryos where *gfp::glo-1* was targeted for degradation, autofluorescent gut granules were no longer basally enriched (Fig 13C). We quantified gut granule localization and found that most were localized apically in the *intDEG; gfp::glo-1* strain (Fig 13D–E), suggesting that GLO-1 activity mediates the basal localization of gut granules. The normal morphology and distribution of WHT-2 in *intDEG; gfp::glo-1* E16 stage embryos strongly suggests that degradation of GLO-1 does not disrupt the gut granule localization and function of WHT-2 in gut granule positioning (Fig S3).

Rab7 directs endolysosome motility and GLO-1 activity can repress the association of RAB-7 with gut granules [20, 21, 32]. We found that the localization of RAB-7 to gut granules was slightly elevated in *intDEG; gfp::glo-1* embryos (Fig 13F–G) and that *rab-7(RNAi)* suppressed the apical mislocalization of gut granules in *intDEG; gfp::glo-1* embryos. These observations are consistent with RAB-7 directing the apical positioning of gut granules when GLO-1 is targeted for degradation (Fig 13D–E).

Discussion

Organelle positioning during epithelial polarization

Coincident with apico-basal polarization of the cell cortex and the establishment of epithelial cell-cell junctions within the intestinal primordium [12], our work shows that *C. elegans* intestinal cells establish dramatic asymmetries in organelle positioning along the apico-basal axis. Along with the nucleus, organelles composing the conventional endolysosomal pathway were localized near the apical cortex (Fig 1). Conversely, gut granules, yolk platelets, and lipid droplets were highly enriched basally (Fig 1). Golgi and mitochondria, while basally biased, were more uniformly distributed along the apico-basal axis (Fig 1). None of these organelles had a polarized distribution in E8 stage intestinal cells (Fig 2), indicating that the cytoplasm undergoes a significant reorganization during epithelial polarization.

Epithelial polarization of *C. elegans* intestinal cells is controlled by PAR-3, which regulates multiple aspects of cortical polarization, including formation of an apically localized MTOC and the organization of apical cell-cell junctions [13, 75]. However, unlike its roles at the cell cortex, PAR-3 is not required to generate asymmetries in organelle position along the apico-basal axis at the time of epithelial polarization (Fig 3). This is in contrast to the requirement for PAR-3 in the apical positioning of endosomes in adult *C. elegans* intestinal cells [10], indicating that PAR-3 is necessary for the maintenance but not establishment of asymmetric organelle positioning in intestinal cells. In the *C. elegans* zygote PAR-3 directs the asymmetric positioning of early endosomes [55], whereas PAR-3 is not required for asymmetric localization of early endosomes in polarizing intestinal cells (Fig 3), highlighting the different mechanisms used to position organelles during development.

The non-random, asymmetric positioning of organelles along the apico-basal axis suggest active mechanisms control organelle localization. What then are the functional consequences of the constellation of organelle asymmetries created during epithelial polarization? The close association of conventional endolysosomal organelles with the nascent apical cell cortex might support membrane trafficking pathways known to establish and maintain epithelial polarity [7–9]. The apical migration of nuclei could act to restrict the interactions between apically and basally positioned organelles, similar to how the perinuclear cloud of endosomes in nonepithelial cells is segregated from peripheral organelles [21]. The three basally enriched organelles, gut granules, yolk platelets, and lipid droplets, function in different aspects of lipid metabolism [76, 77]. It is therefore possible that being restricted to the same region of the cytoplasm facilitates exchange between similarly positioned organelles.

Mechanisms directing gut granule positioning

The asymmetric distribution of basally enriched gut granules and yolk platelets was disrupted in *unc-83(−)* mutants (Fig 1). UNC-83 is a nuclear envelope localized KASH subunit of the conserved LINC complex [14], which contributes to the apical migration of nuclei during intestinal cell polarization by coupling nuclei to the cytoskeleton [14, 78, 79]. Nuclei become centrally positioned within polarizing intestinal cells when UNC-83 function

is disrupted (Fig 1) [14], which likely explains how *unc-83(−)* disrupts apico-basal organelle asymmetry. This is in contrast to another *C. elegans* KASH protein ANC-1, which alters ER, mitochondrial, and lipid droplet positioning in hypodermal cells independently of its role in nuclear anchoring [80]. During the polarization of intestinal cells, gut nuclei occupy a significant portion of the cytoplasm and when positioned near the midline likely contributes to basal organelle localization by excluding organelles from the apical domain. Gut granule and yolk platelet apico-basal polarity is lost and they gain access to the apical domain when nuclear positioning is disrupted. Notably, lipid droplets remain basally localized in *unc-83(−)* mutants (Fig 1), indicating that their distribution is mediated by a different process. This could result from active basal transport, by forming stable contacts with basally anchored organelles, or by becoming clustered after being basally positioned so that they cannot pass nuclei [81, 82]. Endosomes and endolysosomes remain apically positioned when nuclear migration is disrupted. *unc-83(−)* does not obviously disrupt the apical MTOC or organization of the microtubule array [75], and based on the well-documented role of microtubules in endosome motility in other cell types [3, 12, 21, 83, 84], apico-basally oriented microtubules likely contribute to the positioning of apical endosomes during epithelial polarization.

The loss of gut granule apico-basal polarity in *unc-83(−)* is consistent with gut granule localization being the result of random diffusion and exclusion from the apical domain due to nuclear position. However, if passive mechanisms position gut granules, then we would not expect alterations in gut granule protein and lipid composition to disrupt their apico-basal polarization. It is therefore notable that mutations in BLOC-1 and HOPS complex subunits, which have conserved functions in LRO protein trafficking [51, 63], disrupted apico-basal gut granule polarity, without altering nuclear positioning (Fig 7). Little is known regarding the role of LRO biogenesis factors in LRO positioning, likely because most LROs that have been studied to date do not exhibit asymmetric positioning similar to gut granules. However, the LRO biogenesis complexes HOPS and BLOC-3 promote the proper positioning of conventional lysosomes [85, 86], albeit via unknown mechanisms. Regardless of whether BLOC-1 and HOPS directly control LRO motility or indirectly act to deliver cargo to gut granules that function in their positioning, their involvement in gut granule localization strongly suggests that gut granules are actively positioned basally along with being excluded from the apical domain by nuclei.

Our work shows that *wht-2* and *wht-7* have essential roles in gut granule positioning. However, unlike BLOC-1 and HOPS mutants, which no longer show apico-basal polarization of gut granules (Fig 7), *wht-2(−)* and *wht-7(−)* mutants show a complete and specific reversal of gut granule positional asymmetry (Fig. 4), suggesting that WHT-2 and WHT-7 function differently than canonical trafficking factors.

wht-2 and *wht-7* encode WHT/ABCG half-transporters that are part of the White subfamily of ABC proteins, which actively translocate a diverse array of substrates across cellular membranes [59]. While ABCG transporters can function as homodimers [64], our genetic experiments point to WHT-2/WHT-7 heterodimers controlling gut granule apico-basal polarity. Consistent with WHT-2 and WHT-7 acting together, the *wht-2(−)* and *wht-7(−)* single and *wht-2(−); wht-7(−)* double mutants showed identical effects on gut granule

positioning (Fig 9). While the single mutants had little effect on gut granule positioning, combining WHT-2 and WHT-7 Walker A motif ATPase mutants led to the apical enrichment of gut granules (Fig 10). Due to the composite nature of ATP binding sites created by each subunit when ABCG proteins dimerize [69], this result strongly suggests that WHT-2 and WHT-7 function as a heterodimer. If WHT-2 and WHT-7 act as homodimers to direct gut granule localization, then disrupting their ATPase activity should alter gut granule positioning similar to the deletion mutants, which they did not (Fig 10) [69].

There is precedent for individual ABCG transporters functioning as heterodimers as well as homodimers [87]. Our analysis of *wht-2(−)* and *wht-7(−)* single mutants indicates that WHT-2 has WHT-7 independent functions in gut granule biogenesis. Whereas *wht-2(−)* disrupts the formation of crystalline gut granule contents (Fig 9), exhibits genetic interactions with *glo-3(−)* [27], and leads to the loss of the GLO-1 Rab from gut granules (Fig 11), *wht-7(−)* does not have any of these effect (Figs 9, 11, S2). Moreover, WHT-2 is trafficked to gut granules in the absence of WHT-7 (Fig 9), where it could function independently of WHT-7. We therefore propose that WHT-2 acts as a homodimer in gut granule biogenesis and as part of a WHT-2/WHT-7 heterodimer in gut granule positioning.

The significant apical enrichment of gut granules in WHT-2(K74R); WHT-7(K105R) Walker A motif mutants strongly suggests that WHT-2 and WHT-7 function as a membrane transporter in gut granule positioning (Fig 10). ABCG transporters bind substrates at the interface between the monomers [88], suggesting the possibility that WHT-2 transporter specificity is altered by whether it homo or heterodimerizes. This would be similar to the *Drosophila* ABCG protein White, which has been proposed to transport different substrates into lysosome-related pigment granules depending upon whether it heterodimerizes with Scarlet or Brown [89]. While the substrates transported by WHT-2/WHT-7 impacting gut granule positioning are unknown, homologous human ABCG transporters transport a variety of lipids [90], which are known to be key drivers of cell polarity due to their effects on membrane architecture [91]. Additionally, changes in membrane lipid composition can directly impact microtubule motor function to alter organelle position [92].

When gut granule protein trafficking is disrupted by mutations in subunits of the BLOC-1 (*glo-2*), BLOC-3-like (*glo-3*), and HOPS (*vps-18*) complexes [60], some gut granules became localized apically, however not to the same levels as seen in *wht-2(−)* and *wht-7(−)* mutants (Fig 7). Moreover, *wht-2(−)* and *wht-7(−)* mutants did not show any defects in the localization of gut granule proteins and their gut granules did not take on any of the characteristics of apically localized conventional endosomes (Figs 6 and 9). This suggests that the *wht* mutants do not generally alter gut granule formation to cause their mispositioning.

Altering the lipid composition of lysosomal membranes can promote lysophagy, the targeting and destruction of lysosomes by autophagy [93]. Disrupted WHT-2/WHT-7 transporter activity could similarly change gut granule membranes, leading to their clearance. If gut granules were placed within autophagosomes they could be targeted apically in order to fuse with conventional lysosomes and be degraded. However, gut granules are abundant in later stage embryos [27] and RAB-7, which associates with

autophagosomes [94], was not detected on gut granules in wh*t-2(−)* mutants (Fig 6). We therefore think it likely that WHT-2 and WHT-7 affect a specific process impacting gut granule positioning rather than generally altering gut granule formation or causing their degradation in apical endolysosomes.

WHT-2 controls gut granule positioning through Rabs

The phenotypes of *wht-2(−)* and *wht-7(−)* loss-of-function mutants indicate that WHT-2/WHT-7 functions to prevent the apical accumulation of gut granules. During epithelial polarization, gut granules, like early endosomes and endolysosomes, might contain factors with the potential to promote their apical positioning. In this scenario, WHT-2/WHT-7 could be directly or indirectly inhibiting these factors and/or promoting the activity of factors directing gut granules basally. Alternatively, gut granules might lack factors directing apico-basal positioning and when WHT-2/WHT-7 activity is disrupted, they acquire a factor mediating their apical localization.

Our studies suggest that GLO-1, a Rab32/38 homolog [15], acts downstream of WHT-2/WHT-7 to direct the polarized distribution of gut granules. Strikingly, ectopic expression of GLO-1 led to the restoration of basal gut granules in *wht-2(−)* and *wht-7(−)* mutants and the targeted degradation of GLO-1 led to the apical accumulation of gut granules (Figs 12 and 13). In addition, the loss of GLO-1 from gut granules immediately preceded their apical mispositioning in *wht-2(−)* mutants (Fig 11). Vertebrate Rab32/38 functions in LRO motility and physically interacts with myosin [26, 95, 96], supporting the possibility that GLO-1 directs the basal localization of gut granules.

GLO-3 is a subunit of the likely GLO-1 activating guanine nucleotide exchange factor (GEF) and gut granules in *glo-3(kx38)*, like *wht-2(−)* mutants, lack GLO-1 [32]. If gut granule associated GLO-1 functions in gut granule positioning, then why do gut granules not become apically enriched in *glo-3(−)* mutants (Fig 7)? We believe that the different functions of WHT-2 and GLO-3 in GLO-1 activation and gut granule biogenesis could explain their different roles in gut granule positioning. Inactive GLO-1(GDP) likely accumulates when GLO-3/GEF activity is disrupted, whereas WHT-2 has a GEF independent role in the association of GLO-1 with gut granules [27]. The loss of active GLO-1(GTP) disrupts gut granule biogenesis, resulting in *glo-3(−)* mutants having significant alterations in gut granule protein composition, a phenotype not displayed by *wht-2(−)* [27]. It is therefore possible that defects in gut granule biogenesis caused by *glo-3(−)* produce gut granules lacking factors promoting their apical accumulation. These factors would be present when WHT-2 function is disrupted due to a more limited role of WHT-2 in gut granule biogenesis. Consistent with this idea, WHT-2 does not appear to impact GLO-1 localization to gut granules until the E16 stage (Fig 11), which is after the initiation of gut granule biogenesis [27]. If the GLO-1 Rab regulates gut granule biogenesis in E8 and earlier stage intestinal cells before transitioning to regulating gut granule positioning at the E16 stage, then *wht-2(−)* could specifically impact GLO-1 function in organelle localization during epithelial polarization.

Our data support the model that WHT-2 promotes the localization of GLO-1 to E16 stage gut granules, which in turn prevents their apical localization. Our results also point to

WHT-2 functioning as a membrane transporter with WHT-7 to position gut granules (Figs 10 and 12). It is therefore surprising that *wht-7(−)* does not cause the loss of GLO-1 from E16 gut granules, in contrast to *wht-2(−)* (Fig 11). It is important to note that we analyzed the steady state localization of GLO-1, leaving open the possibility that *wht-7(−)* is altering dynamics of GLO-1 localization that are important to its activity. For example, there might be an increased rate of GLO-1 cycling on and off gut granules, decreasing the duration of GLO-1 association, either of which could impact GLO-1 function. Alternatively, *wht-7(−)* might not disrupt the association of GLO-with gut granules, but instead lead to decreased nucleotide exchange and activation of GLO-1. In either scenario WHT-2 homodimers might partially compensate for the loss of WHT-7 to support the steady state localization of GLO-1 in *wht-7(−)*. It is important to note that our data do not exclude the possibility that WHT-7 acts independently of WHT-2 and GLO-1 to impact gut granule positioning. However, this seems unlikely in light of the synthetic genetic interactions between WHT-2 and WHT-7 ATPase mutants and the suppression of both *wht-2(−)* and *wht-7(−)* by the ectopic expression of GLO-1 (Figs 10 and 12).

Our work also points to a role for the endolysosomal RAB-7 in gut granule mispositioning. When WHT-2 or GLO-1 activity was disrupted, *rab-7(RNAi)* potently suppressed the apical mislocalization of gut granules (Figs 7 and 13). While not as strong, *rab-7(RNAi)* also suppressed *wht-7(−)* (Fig 7). Interestingly, when GLO-1 was targeted for degradation, RAB-7 became associated with some apically mispositioned gut granules (Fig 13). Rab7 is known to mediate the bidirectional transport of endolysosomes along microtubules through its recruitment of kinesin and dynein [84, 97], suggesting the possibility that mislocalized RAB-7 could direct the apical directed movement of gut granules along the polarized microtubule array that is present in E16 stage intestinal cells [12].

The asymmetries in organelle positioning associated with epithelial polarization have rarely been documented and are largely unexplored. Polarizing *C. elegans* intestinal cells represent an attractive system to investigate the mechanisms that generate and the consequences of organelle asymmetries. While our studies of WHT-2/WHT-7 and the GLO-1 and RAB-7 GTPases provide insights into asymmetric gut granule positioning, the mechanisms directing the apical accumulation of conventional endosomes and the basal localization of lipid droplets in polarizing epithelial cells are currently unknown and warrant further study.

Supplementary Material

Refer to Web version on PubMed Central for supplementary material.

Acknowledgements

We thank Jon Audhya, Barth Grant, Kerry Kornfeld, Fritz Mueller, Jeremy Nance, and Xiochen Wang for strains and antibodies. We thank members of the Hermann lab, Margaret Metz, Deborah Lycan, and Tamily Weissman for helpful discussions. We are grateful to Nicole Brockway for assistance with confocal microscopy. Some of the strains used in this work were provided by the *Caenorhabditis* Genetics Center and the National Bioresource Project for *Caenorhabditis elegans*. This work was supported by the National Institutes of Health (1R15GM120639-01), the National Science Foundation (MCB1612804), the Howard Hughes Medical Institute, and the John S. Rogers Summer Research Program.

References

1. Simons K and Fuller SD. Cell surface polarity in epithelia. Annu Rev Cell Biol, 1985. 1: p. 243–88. [PubMed: 3939606]
2. Pickett MA, Naturale VF, and Feldman JL. A polarizing issue: Diversity in the mechanisms underlying apico-basolateral polarization in vivo. Annu Rev Cell Dev Biol, 2019. 35: p. 285–308. [PubMed: 31461314]
3. Rodriguez-Boulan E and Macara IG. Organization and execution of the epithelial polarity programme. Nat Rev Mol Cell Biol, 2014. 15(4): p. 225–42. [PubMed: 24651541]
4. Taverna E, Gotz M, and Huttner WB. The cell biology of neurogenesis: toward an understanding of the development and evolution of the neocortex. Annu Rev Cell Dev Biol, 2014. 30: p. 465–502. [PubMed: 25000993]
5. Roman-Fernandez A and Bryant DM. Complex polarity: Building multicellular tissues through apical membrane traffic. Traffic, 2016. 17(12): p. 1244–1261. [PubMed: 27281121]
6. Riga A, Castiglioni VG, and Boxem M. New insights into apical-basal polarization in epithelia. Curr Opin Cell Biol, 2020. 62: p. 1–8. [PubMed: 31505411]
7. Apodaca G, Gallo LI, and Bryant DM. Role of membrane traffic in the generation of epithelial cell asymmetry. Nat Cell Biol, 2012. 14(12): p. 1235–43. [PubMed: 23196841]
8. Eaton S and Martin-Belmonte F. Cargo sorting in the endocytic pathway: a key regulator of cell polarity and tissue dynamics. Cold Spring Harb Perspect Biol, 2014. 6(10): p. a016899. [PubMed: 25125399]
9. Mellman I and Nelson WJ. Coordinated protein sorting, targeting and distribution in polarized cells. Nat Rev Mol Cell Biol, 2008. 9(11): p. 833–45. [PubMed: 18946473]
10. Winter JF, Hopfner S, Korn K, Farnung BO, Bradshaw CR, Marsico G, Volkmer M, Habermann B, and Zerial M. *Caenorhabditis elegans* screen reveals role of PAR-5 in RAB-11-recycling endosome positioning and apicobasal cell polarity. Nat Cell Biol, 2012. 14(7): p. 666–76. [PubMed: 22634595]
11. Maduro MF Gut development in *C. elegans*. Semin Cell Dev Biol, 2017. 66: p. 3–11. [PubMed: 28065852]
12. Leung B, Hermann GJ, and Priess JR. Organogenesis of the *Caenorhabditis elegans* intestine. Dev. Biol, 1999. 216(1): p. 114–34. [PubMed: 10588867]
13. Achilleos A, Wehman AM, and Nance J. PAR-3 mediates the initial clustering and apical localization of junction and polarity proteins during *C. elegans* intestinal epithelial cell polarization. Development, 2010. 137(11): p. 1833–1842. [PubMed: 20431121]
14. Starr DA, Hermann GJ, Malone CJ, Fixsen W, Priess JR, Horvitz HR, and Han M. *unc-83* encodes a novel component of the nuclear envelope and is essential for proper nuclear migration. Development, 2001. 128: p. 5039–5050. [PubMed: 11748140]
15. Hermann GJ, Schroeder LK, Hieb CA, Kershner AM, Rabbitts BM, Fonarev P, Grant BD, and Priess JR. Genetic analysis of lysosomal trafficking in *Caenorhabditis elegans*. Mol. Biol. Cell, 2005. 16(7): p. 3273–88. [PubMed: 15843430]
16. Rabbitts BM, Kokes M, Miller NE, Kramer M, Lawrenson AL, Levitte S, Kremer S, Kwan E, Weis AM, and Hermann GJ. *glo-3*, a novel *Caenorhabditis elegans* gene, is required for lysosome-related organelle biogenesis. Genetics, 2008. 180: p. 857–871. [PubMed: 18780725]
17. Zhang H, Abraham N, Khan LA, Hall DH, Fleming JT, and Gobel V. Apicobasal domain identities of expanding tubular membranes depend on glycosphingolipid biosynthesis. Nat Cell Biol, 2011. 13(10): p. 1189–201. [PubMed: 21926990]
18. Chen B, Jiang Y, Zeng S, Yan J, Li X, Zhang Y, Zou W, and Wang X. Endocytic Sorting and Recycling Require Membrane Phosphatidylserine Asymmetry Maintained by TAT-1/CHAT-1. PLOS Genet., 2010. 6(12): p. e1001235. [PubMed: 21170358]
19. Chen CC, Schweinsberg PJ, Vashist S, Mareiniss DP, Lambie EJ, and Grant BD. RAB-10 Is Required for Endocytic Recycling in the *Caenorhabditis elegans* Intestine. Mol. Biol. Cell, 2006. 17(3): p. 1286–97. [PubMed: 16394106]
20. Ballabio A and Bonifacino JS. Lysosomes as dynamic regulators of cell and organismal homeostasis. Nat Rev Mol Cell Biol, 2020. 21(2): p. 101–118. [PubMed: 31768005]

21. Neefjes J, Jongsma MML, and Berlin I. Stop or Go? Endosome Positioning in the Establishment of Compartment Architecture, Dynamics, and Function. Trends Cell Biol, 2017. 27(8): p. 580–594. [PubMed: 28363667]
22. Khatter D, Sindhwani A, and Sharma M. Arf-like GTPase Arl8: Moving from the periphery to the center of lysosomal biology. Cell Logist, 2015. 5(3): p. e1086501. [PubMed: 27057420]
23. Kummel D and Ungermann C. Principles of membrane tethering and fusion in endosome and lysosome biogenesis. Curr Opin Cell Biol, 2014. 29C: p. 61–66.
24. Scott CC, Vacca F, and Gruenberg J. Endosome maturation, transport and functions. Semin Cell Dev Biol, 2014. 31: p. 2–10. [PubMed: 24709024]
25. Trivedi PC, Bartlett JJ, and Pulinilkunnil T. Lysosomal biology and function: Modern view of cellular debris bin. Cells, 2020. 9(5).
26. Park M, Serpinskaya AS, Papalopulu N, and Gelfand VI. Rab32 regulates melanosome transport in Xenopus melanophores by protein kinase a recruitment. Curr Biol, 2007. 17(23): p. 2030–4. [PubMed: 17997311]
27. Voss L, Foster OK, Harper L, Morris C, Lavoy S, Brandt JN, Peloza K, Handa S, Maxfield A, Harp M, King B, Eichten V, Rambo FM, and Hermann GJ. An ABCG transporter functions in Rab localization and lysosome-related organelle biogenesis in *Caenorhabditis elegans*. Genetics, 2020. 214(2): p. 419–445. [PubMed: 31848222]
28. Stiernagle T, Maintenance of C. elegans, in C. elegans: A Practical Approach, Hope I, Editor. 1999, Oxford University Press. p. pp. 51–67.
29. Davis DE, Roh HC, Deshmukh K, Bruinsma JJ, Schneider DL, Guthrie J, Robertson JD, and Kornfeld K. The cation diffusion facilitator gene *cdf-2* mediates zinc metabolism in *Caenorhabditis elegans*. Genetics, 2009. 182(4): p. 1015–33. [PubMed: 19448268]
30. Zhang SO, Box AC, Xu N, Le Men J, Yu J, Guo F, Trimble R, and Mak HY. Genetic and dietary regulation of lipid droplet expansion in Caenorhabditis elegans. Proc Natl Acad Sci U S A, 2010. 107(10): p. 4640–5. [PubMed: 20176933]
31. Levitte S, Salesky R, King B, Coe Smith S, Depper M, Cole M, and Hermann GJ. A Caenorhabditis elegans model of orotic aciduria reveals enlarged lysosome-related organelles in embryos lacking umps-1 function. FEBS J, 2010. 277(6): p. 1420–39. [PubMed: 20148972]
32. Morris C, Foster OK, Handa S, Peloza K, Voss L, Somhegyi H, Jian Y, Vo MV, Harp M, Rambo FM, Yang C, and Hermann GJ. Function and regulation of the Caenorhabditis elegans Rab32 family member GLO-1 in lysosome-related organelle biogenesis. PLoS Genet, 2018. 14(11): p. e1007772. [PubMed: 30419011]
33. Wang S, Tang NH, Lara-Gonzalez P, Zhao Z, Cheerambathur DK, Prevo B, Chisholm AD, Desai A, and Oegema K. A toolkit for GFP-mediated tissue-specific protein degradation in C. elegans. Development, 2017. 144(14): p. 2694–2701. [PubMed: 28619826]
34. Neukomm LJ, Nicot AS, Kinchen JM, Almendinger J, Pinto SM, Zeng S, Doukoumetzidis K, Tronchere H, Payrastre B, Laporte JF, and Hengartner MO. The phosphoinositide phosphatase MTM-1 regulates apoptotic cell corpse clearance through CED-5-CED-12 in C. elegans. Development, 2011. 138(10): p. 2003–14. [PubMed: 21490059]
35. Sato M, Sato K, Fonarev P, Huang CJ, Liou W, and Grant BD. *Caenorhabditis elegans* RME-6 is a novel regulator of RAB-5 at the clathrin-coated pit. Nat Cell Biol, 2005. 7(6): p. 559–69. [PubMed: 15895077]
36. Treusch S, Knuth S, Slaugenhaupt SA, Goldin E, Grant BD, and Fares H. *Caenorhabditis elegans* functional orthologue of human protein h-mucolipin-1 is required for lysosome biogenesis. Proc. Nat. Acad. Sci. (USA), 2004. 13: p. 4483–4488.
37. Liu B, Du H, Rutkowski R, Gartner A, and Wang X. LAAT-1 is the lysosomal lysine/arginine transporter that maintains amino acid homeostasis. Science, 2012. 337(6092): p. 351–4. [PubMed: 22822152]
38. Nakae I, Fujino T, Kobayashi T, Sasaki A, Kikko Y, Fukuyama M, Gengyo-Ando K, Mitani S, Kontani K, and Katada T. The arf-like GTPase Arl8 mediates delivery of endocytosed macromolecules to lysosomes in Caenorhabditis elegans. Mol Biol Cell, 2010. 21(14): p. 2434–42. [PubMed: 20484575]

39. Nance J, Munro EM, and Priess JR. *C. elegans* PAR-3 and PAR-6 are required for apicobasal asymmetries associated with cell adhesion and gastrulation. Development, 2003. 130(22): p. 5339–5350. [PubMed: 13129846]
40. Kamath RS, Martinez-Campos M, Zipperlen P, Fraser AG, and Ahringer J. Effectiveness of specific RNA-mediated interference through ingested double-stranded RNA in Caenorhabditis elegans. Genome Biol, 2001. 2(1): p. RESEARCH0002. [PubMed: 11178279]
41. Moorthy S, Chen L, and Bennet V. *Caenorhabditis elegans* beta-G spectrin is dispensable for the establishemnt of epithelial polarity, but essential for muscular and neuronal function. J. Cell. Biol, 2000. 149: p. 915–930. [PubMed: 10811831]
42. Hadwiger G, Dour S, Arur S, Fox P, and Nonet ML. A monoclonal antibody toolkit for C. elegans. PLOS One, 2010. 5(4): p. e10161. [PubMed: 20405020]
43. Liu F, Thatcher JD, Barral JM, and Epstein HF. Bifunctional glyoxylate cycle protein of Caenorhabditis elegans: a developmentally regulated protein of intestine and muscle. Dev Biol, 1995. 169(2): p. 399–414. [PubMed: 7781887]
44. Schroeder LK, Kremer S, Kramer MJ, Currie E, Kwan E, Watts JL, Lawrenson AL, and Hermann GJ. Function of the *Caenorhabditis elegans* ABC transporter PGP-2 in the biogenesis of a lysosome-related fat storage organelle. Mol. Biol. Cell, 2007. 18(3): p. 995–1008. [PubMed: 17202409]
45. Audhya A, Desai A, and Oegema K. A role for Rab5 in structuring the endoplasmic reticulum. J. Cell Biol, 2007. 178(1): p. 43–56. [PubMed: 17591921]
46. Eisenhut RJ, Knox D, and Hermann GJ. Characterization of a conserved apoptotic marker expressed in *Caenorhabditis elegans* phagocytic cells. Biochem Biophys Res Commun, 2005. 335(4): p. 1231–8. [PubMed: 16115612]
47. Fridolfsson HN, Herrera LA, Brandt JN, Cain NE, Hermann GJ, and Starr DA, Genetic analysis of nuclear migration and anchorage to study LINC complexes during development of Caenorhabditis elegans., in The LINC Complexes: Methods and Protocols. 2018, Springer. p. 163–180.
48. Rizk A, Paul G, Incardona P, Bugarski M, Mansouri M, Niemann A, Ziegler U, Berger P, and Sbalzarini IF. Segmentation and quantification of subcellular structures in fluorescence microscopy images using Squassh. Nat Protoc, 2014. 9(3): p. 586–96. [PubMed: 24525752]
49. Schindelin J, Arganda-Carreras I, Frise E, Kaynig V, Longair M, Pietzsch T, Preibisch S, Rueden C, Saalfeld S, Schmid B, Tinevez JY, White DJ, Hartenstein V, Eliceiri K, Tomancak P, and Cardona A. Fiji: an open-source platform for biological-image analysis. Nat Methods, 2012. 9(7): p. 676–82. [PubMed: 22743772]
50. Sulston JE Post-embryonic development in the ventral cord of Caenorhabditis elegans. Philos. Trans. R. Soc. Lond. B. Biol. Sci, 1976. 275: p. 287–297. [PubMed: 8804]
51. Hermann GJ, Scavarda E, Weis AM, Saxton DS, Thomas LL, Salesky R, Somhegyi H, Curtin TP, Barrett A, Foster OK, Vine A, Erlich K, Kwan E, Rabbitts BM, and Warren K. C. elegans BLOC-1 functions in trafficking to lysosome-related gut granules. PLoS One, 2012. 7(8): p. e43043. [PubMed: 22916203]
52. Bone CR and Starr DA. Nuclear migration events throughout development. Journal of Cell Science, 2016. 129(10): p. 1951–1961. [PubMed: 27182060]
53. Burakov AV and Nadezhdina ES. Association of nucleus and centrosome: magnet or velcro? Cell Biol Int, 2013. 37(2): p. 95–104. [PubMed: 23319360]
54. Lang CF and Munro E. The PAR proteins: from molecular circuits to dynamic self-stabilizing cell polarity. Development, 2017. 144(19): p. 3405–3416. [PubMed: 28974638]
55. Andrews R and Ahringer J. Asymmetry of early endosome distribution in *C. elegans* embryos. PLoS One, 2007. 2(6): p. e493. [PubMed: 17551574]
56. Kemphues KJ, Priess JR, Morton DG, and Cheng N. Identification of genes required for cytoplasmic localization in the early *C. elegans* embryos. Cell, 1988. 52: p. 311–320. [PubMed: 3345562]
57. Thompson O, Edgley M, Strasbourger P, Flibotte S, Ewing B, Adair R, Au V, Chaudhry I, Fernando L, Hutter H, Kieffer A, Lau J, Lee N, Miller A, Raymant G, Shen B, Shendure J, Taylor J, Turner EH, Hillier LW, Moerman DG, and Waterston RH. The million mutation project: a new

approach to genetics in *Caenorhabditis elegans*. Genome Res, 2013. 23(10): p. 1749–62. [PubMed: 23800452]

58. Sarkadi B, Homolya L, Szakacs G, and Varadi A. Human multidrug resistance ABCB and ABCG transporters: participation in a chemoimmunity defense system. Physiol Rev, 2006. 86(4): p. 1179–236. [PubMed: 17015488]
59. Sheps JA, Ralph S, Zhao Z, Baillie DL, and Ling V. The ABC transporter gene family of *Caenorhabditis elegans* has implications for the evolutionary dynamics of multidrug resistance in eukaryotes. Genome Biol, 2004. 5(3): p. R15. [PubMed: 15003118]
60. Bowman SL, Bi-Karchin J, Le L, and Marks MS. The road to LROs: insights into lysosome-related organelles from Hermansky-Pudlak syndrome and other rare diseases. Traffic, 2019. 20: p. 404–435. [PubMed: 30945407]
61. Sato K, Norris A, Sato M, and Grant BD, C. elegans as a model for membrane traffic (April 25, 2014), in Wormbook, T.C.e.R. Community, Editor. 2014.
62. Dumas JJ, Merithew E, Sudharshan E, Rajamani D, Hayes S, Lawe D, Corvera S, and Lambright DG. Multivalent endosome targeting by homodimeric EEA1. Mol Cell, 2001. 8(5): p. 947–58. [PubMed: 11741531]
63. Delahaye JL, Foster OK, Vine A, Saxton DS, Curtin TP, Somhegyi H, Salesky R, and Hermann GJ. *Caenorhabditis elegans* HOPS and CCZ-1 mediate trafficking to lysosome-related organelles independently of RAB-7 and SAND-1. Mol Biol Cell, 2014. 25(7): p. 1073–96. [PubMed: 24501423]
64. Tarr PT, Tarling EJ, Bojanic DD, Edwards PA, and Baldan A. Emerging new paradigms for ABCG transporters. Biochim Biophys Acta, 2009. 1791(7): p. 584–93. [PubMed: 19416657]
65. Taylor NMI, Manolaridis I, Jackson SM, Kowal J, Stahlberg H, and Locher KP. Structure of the human multidrug transporter ABCG2. Nature, 2017. 546(7659): p. 504–509. [PubMed: 28554189]
66. Henriksen U, Gether U, and Litman T. Effect of Walker A mutation (K86M) on oligomerization and surface targeting of the multidrug resistance transporter ABCG2. J Cell Sci, 2005. 118(Pt 7): p. 1417–26. [PubMed: 15769853]
67. Ozvegy C, Varadi A, and Sarkadi B. Characterization of drug transport, ATP hydrolysis, and nucleotide trapping by the human ABCG2 multidrug transporter. Modulation of substrate specificity by a point mutation. J Biol Chem, 2002. 277(50): p. 47980–90. [PubMed: 12374800]
68. Zhang DW, Graf GA, Gerard RD, Cohen JC, and Hobbs HH. Functional asymmetry of nucleotide-binding domains in ABCG5 and ABCG8. J Biol Chem, 2006. 281(7): p. 4507–16. [PubMed: 16352607]
69. Eckenstaler R and Benndorf RA. 3D structure of the transporter ABCG2-What's new? Br J Pharmacol, 2020. 177(7): p. 1485–1496. [PubMed: 31985041]
70. Hegyi Z and Homolya L. Functional cooperativity between ABCG4 and ABCG1 isoforms. Plos One, 2016. 11(5).
71. Cserepes J, Szentpetery Z, Seres L, Ozvegy-Laczka C, Langmann T, Schmitz G, Glavinas H, Klein I, Homolya L, Varadi A, Sarkadi B, and Elkind NB. Functional expression and characterization of the human ABCG1 and ABCG4 proteins: indications for heterodimerization. Biochem Biophys Res Commun, 2004. 320(3): p. 860–7. [PubMed: 15240127]
72. Gao M, Cui HR, Loe DW, Grant CE, Almquist KC, Cole SPC, and Deeley RG. Comparison of the functional characteristics of the nucleotide binding domains of multidrug resistance protein 1. Journal of Biological Chemistry, 2000. 275(17): p. 13098–13108.
73. Perria CL, Rajamanickam V, Lapinski PE, and Raghavan M. Catalytic site modifications of TAP1 and TAP2 and their functional consequences. Journal of Biological Chemistry, 2006. 281(52): p. 39839–39851.
74. Procko E, Ferrin-O'Connell I, Ng SL, and Gaudet R. Distinct structural and functional properties of the ATPase sites in an asymmetric ABC transporter. Molecular Cell, 2006. 24(1): p. 51–62. [PubMed: 17018292]
75. Feldman JL and Priess JR. A role for the centrosome and PAR-3 in the hand-off of MTOC function during epithelial polarization. Curr Biol, 2012. 22(7): p. 575–82. [PubMed: 22425160]
76. Srinivasan S Regulation of body fat in *Caenorhabditis elegans*. Annu Rev Physiol, 2015. 77: p. 161–78. [PubMed: 25340962]

77. Watts JL and Ristow M. Lipid and carbohydrate metabolism in *Caenorhabditis elegans*. Genetics, 2017. 207(2): p. 413–446. [PubMed: 28978773]

78. Starr DA A network of nuclear envelope proteins and cytoskeletal force generators mediates movements of and within nuclei throughout Caenorhabditis elegans development. Exp Biol Med (Maywood), 2019. 244(15): p. 1323–1332. [PubMed: 31495194]

79. Wong X, Loo TH, and Stewart CL. LINC complex regulation of genome organization and function. Curr Opin Genet Dev, 2021. 67: p. 130–141. [PubMed: 33524904]

80. Hao H, Kalra S, Jameson LE, Guerrero LA, Cain NE, Bolivar J, and Starr DA. The Nesprin-1/−2 ortholog ANC-1 regulates organelle positioning in C. elegans independently from its KASH or actin-binding domains. Elife, 2021. 10.

81. Kilwein MD and Welte MA. Lipid droplet motility and organelle contacts. Contact (Thousand Oaks), 2019. 2.

82. Olzmann JA and Carvalho P. Dynamics and functions of lipid droplets. Nat Rev Mol Cell Biol, 2019. 20(3): p. 137–155. [PubMed: 30523332]

83. Bornens M Organelle positioning and cell polarity. Nat Rev Mol Cell Biol, 2008. 9(11): p. 874–86. [PubMed: 18946476]

84. Cabukusta B and Neefjes J. Mechanisms of lysosomal positioning and movement. Traffic, 2018. 19(10): p. 761–769. [PubMed: 29900632]

85. Falcon-Perez JM, Nazarian R, Sabatti C, and Dell'Angelica EC. Distribution and dynamics of Lamp1-containing endocytic organelles in fibroblasts deficient in BLOC-3. J Cell Sci, 2005. 118(Pt 22): p. 5243–55. [PubMed: 16249233]

86. Galmes R, ten Brink C, Oorschot V, Veenendaal T, Jonker C, van der Sluijs P, and Klumperman J. Vps33B is required for delivery of endocytosed cargo to lysosomes. Traffic, 2015. 16(12): p. 1288–305. [PubMed: 26403612]

87. Kerr ID, Haider AJ, and Gelissen IC. The ABCG family of membrane-associated transporters: you don't have to be big to be mighty. Br J Pharmacol, 2011. 164(7): p. 1767–79. [PubMed: 21175590]

88. Banerjee A, Moreno A, Pata J, Falson P, and Prasad R. ABCG: a new fold of ABC exporters and a whole new bag of riddles! Adv Protein Chem Struct Biol, 2021. 123: p. 163–191. [PubMed: 33485482]

89. Mackenzie SM, Howells AJ, Cox GB, and Ewart GD. Sub-cellular localization of the White/Scarlet ABC transporter to pigment granule membranes within the compund eye of *Drosophila melanogaster*. Genetica, 2000. 108: p. 239–252. [PubMed: 11294610]

90. Neumann J, Rose-Sperling D, and Hellmich UA. Diverse relations between ABC transporters and lipids: An overview. Biochim Biophys Acta Biomembr, 2017. 1859(4): p. 605–618. [PubMed: 27693344]

91. Vaidziulyte K, Coppey M, and Schauer K. Intracellular organization in cell polarity - placing organelles into the polarity loop. J Cell Sci, 2019. 132(24).

92. Roney JC, Li S, Farfel-Becker T, Huang N, Sun T, Xie Y, Cheng XT, Lin MY, Platt FM, and Sheng ZH. Lipid-mediated motor-adaptor sequestration impairs axonal lysosome delivery leading to autophagic stress and dystrophy in Niemann-Pick type C. Dev Cell, 2021. 56: p. in press.

93. Papadopoulos C and Meyer H. Detection and Clearance of Damaged Lysosomes by the Endo-Lysosomal Damage Response and Lysophagy. Curr Biol, 2017. 27(24): p. R1330–R1341. [PubMed: 29257971]

94. Lorincz P and Juhasz G. Autophagosome-lysosome fusion. J Mol Biol, 2020. 432(8): p. 2462–2482. [PubMed: 31682838]

95. Bultema JJ, Boyle JA, Malenke PB, Martin FE, Dell'Angelica EC, Cheney RE, and Di Pietro SM. Myosin Vc Interacts with Rab32 and Rab38 Proteins and Works in the Biogenesis and Secretion of Melanosomes. Journal of Biological Chemistry, 2014. 289(48): p. 33513–33528.

96. Hume AN, Wilson MS, Ushakov DS, Ferenczi MA, and Seabra MC. Semi-automated analysis of organelle movement and membrane content: understanding rab-motor complex transport function. Traffic, 2011. 12(12): p. 1686–701. [PubMed: 21920004]

97. Pu J, Guardia CM, Keren-Kaplan T, and Bonifacino JS. Mechanisms and functions of lysosome positioning. Journal of Cell Science, 2016. 129(23): p. 4329–4339. [PubMed: 27799357]

Highlights consisting of bullet points that convey the core findings of the article:

- Organelles develop apico-basal polarity during epithelial polarization
- Cytoplasmic polarization of intestinal cells does not require the PAR polarity system
- Nuclear positioning directs the asymmetric localization of some endosomal organelles
- Lysosome-related organelle positioning requires WHT-2 and WHT-7 ABCG transporters
- Rab GTPases direct organelle localization downstream of WHT-2 and WHT-7

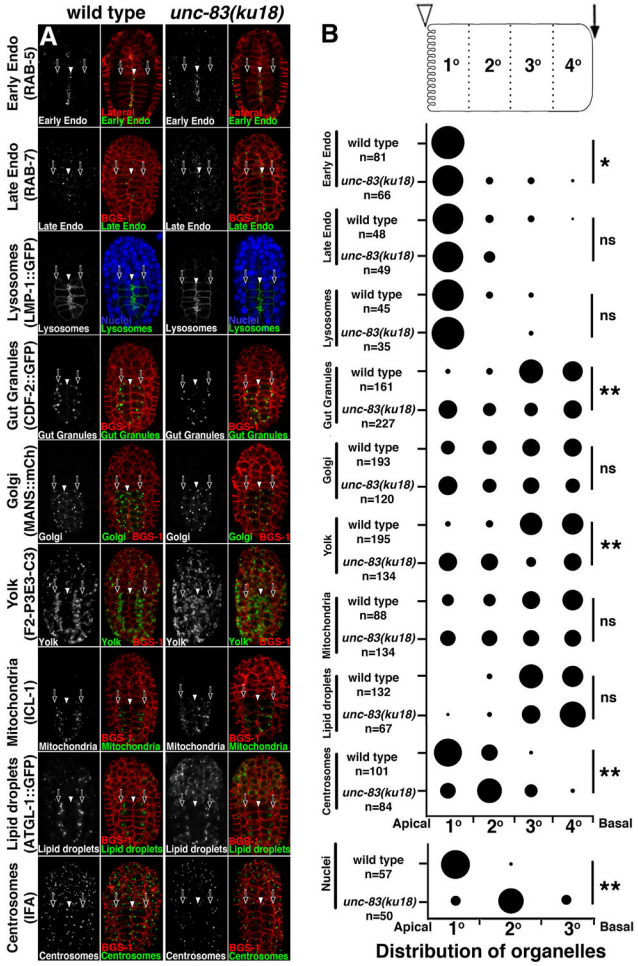

Figure 1. Organelles are asymmetrically positioned in polarizing intestinal epithelial cells.

(A) Organelles in wild type or *unc-83(ku18)* E16 stage embryos were marked with antibodies or fluorescent proteins. To identify the apical and basal domains of intestinal cells at this stage, embryos were stained with a monoclonal antibody that labels the lateral domain of epithelial cells, antibodies to BGS-1, which labels the cell cortex, or DAPI to mark nuclei. Co-stained embryos were imaged with confocal microscopy. Single confocal optical sections acquired at the focal plane that contains the majority of intestinal nuclei are shown. The white arrowhead marks the midline/apical domain and the black arrows denote the basal domain of the intestinal cells. Embryos are 50μm in length and are oriented so that the anterior is at the top and the posterior is at the bottom of each panel. (B) To quantify organelle position, intestinal cells were divided into 3 or 4 equally sized quadrants along the apical basal axis. The number of organelles within each quadrant was scored. Only organelles present within the same focal plane as the nucleus were analyzed. The position of organelles within 8–12 individual intestinal cells was scored in 5–10 embryos of each genotype. The total number of organelles scored is listed below the genotype. In the graph, the area of the circle represents the proportion of organelles located within each quadrant. A Fisher's exact test followed by a Bonferroni correction was used to compare the distribution of each type of organelle between wild type and *unc-83(ku18)* (ns represents a $p > 0.05$, * represents a $p \leq 0.05$, and ** represents a $p \leq 0.001$).

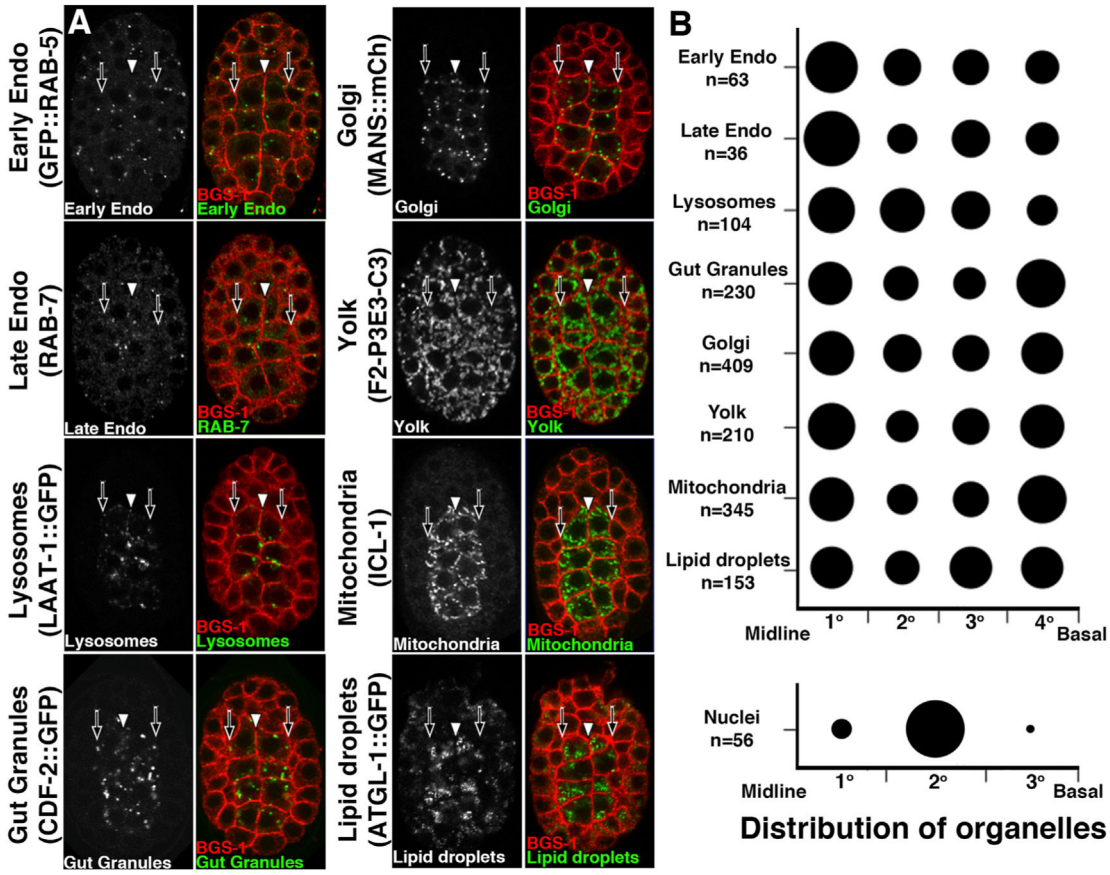

Figure 2. Organelles are not asymmetrically positioned in intestinal cells prior to epithelial polarization.

(A) Wild-type E8 stage embryos were stained with antibodies to the cortical protein BGS-1 and organelles were marked with GFP tagged proteins or antibodies. Embryos were imaged with confocal microscopy, single optical sections are shown, and white arrowheads and black arrows mark the midline and basal intestinal cell domains, respectively. (B) The position of organelles within individual intestinal cells was scored as described in the legend for Figure 1. The area of the circles represents the proportion of organelles located within each quadrant.

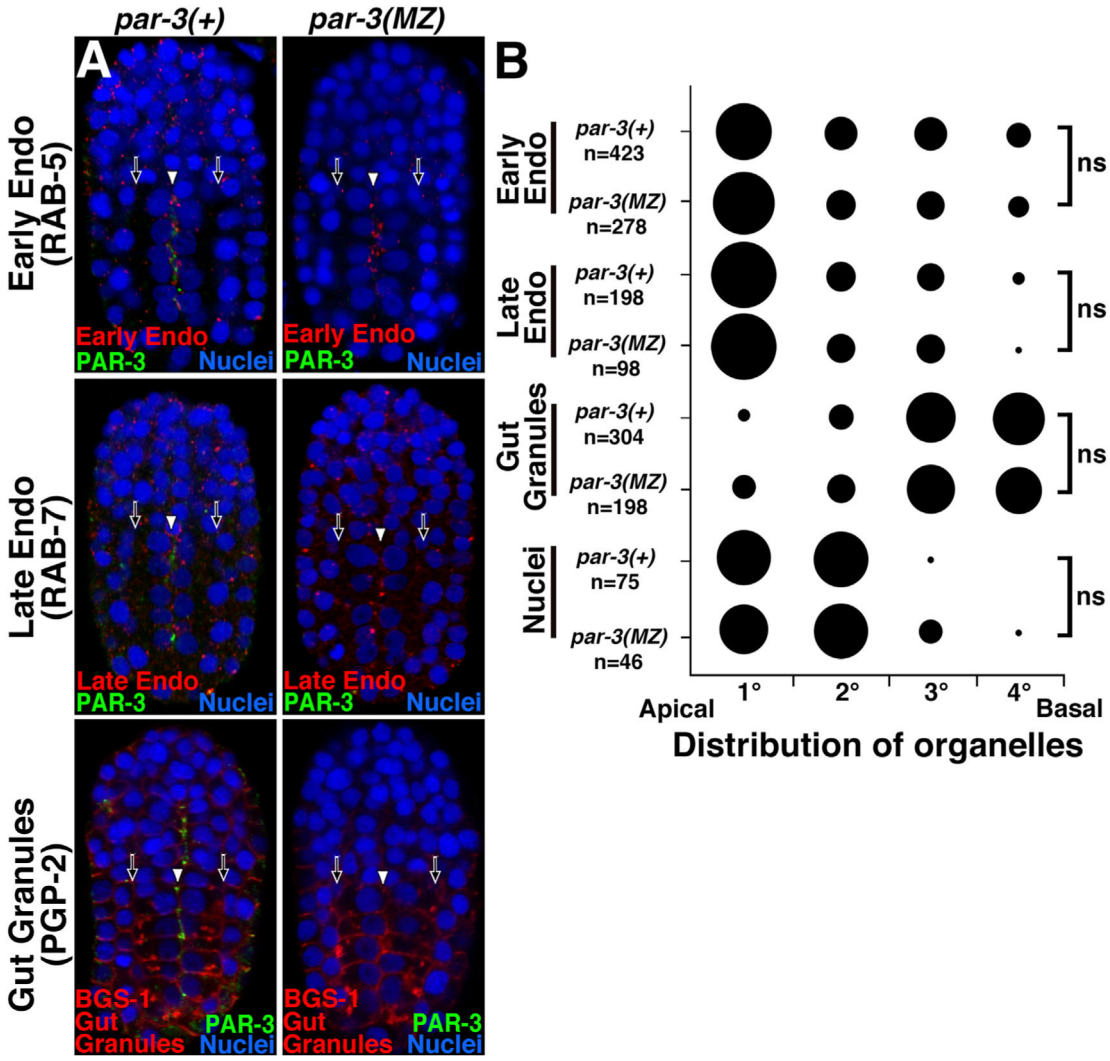

Figure 3. Asymmetric organelle positioning does not require PAR-3.

(A) Wild-type or *par-3(MZ)* E16 stage embryos were stained with the indicated antibodies and DAPI to mark nuclei and imaged with confocal microscopy. Single optical sections are shown, and white arrowheads and black arrows mark the apical and basal intestinal cell domains, respectively. (B) The position of organelles within individual intestinal cells was scored as described in the legend for Figure 1. The area of the circles represents the proportion of organelles located within each quadrant. A Fisher's exact test was used to compare the distribution of each type of organelle between wild type and *par-3(MZ)* (ns represents a $p > 0.05$).

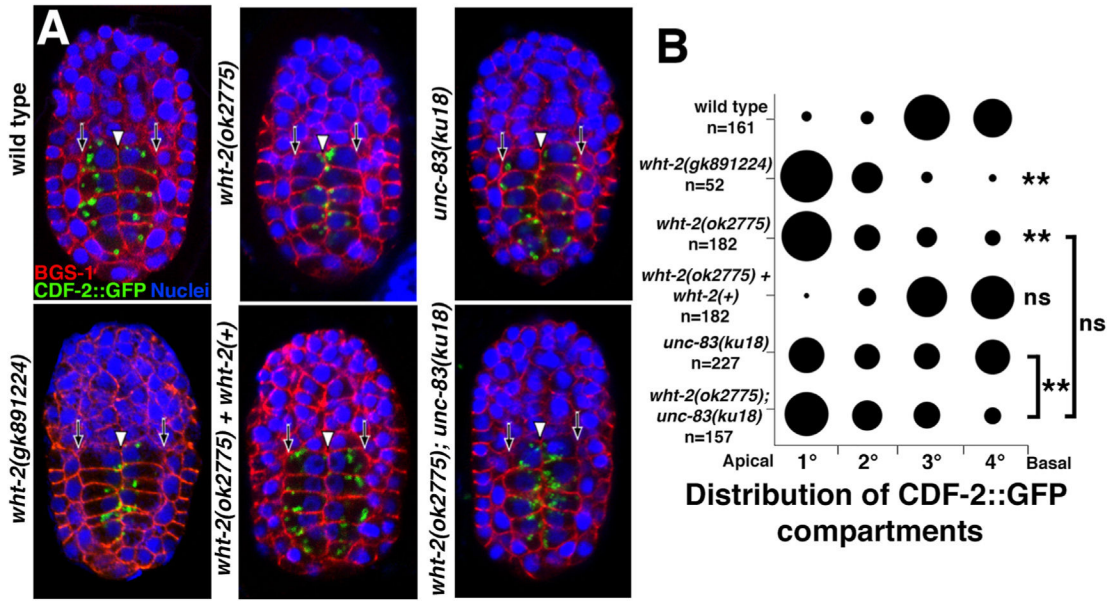

Figure 4. CDF-2::GFP marked organelles are positioned apically rather than basally in *wht-2(−)* mutants.

E16 stage embryos expressing CDF-2::GFP were stained with BGS-1 to mark the cell cortex and DAPI to mark nuclei. Single optical sections are shown, and white arrowheads and black arrows mark the apical and basal intestinal cell domains, respectively. (B) The position of organelles within individual intestinal cells was scored as described in the legend for Figure 1. The area of the circles represents the proportion of organelles located within each quadrant. A Fisher's exact test followed by a Bonferroni correction was used to compare the distribution of each type of organelle between the mutant and wild type unless otherwise noted (ns represents a $p > 0.05$ and ** represents a $p \leq 0.001$).

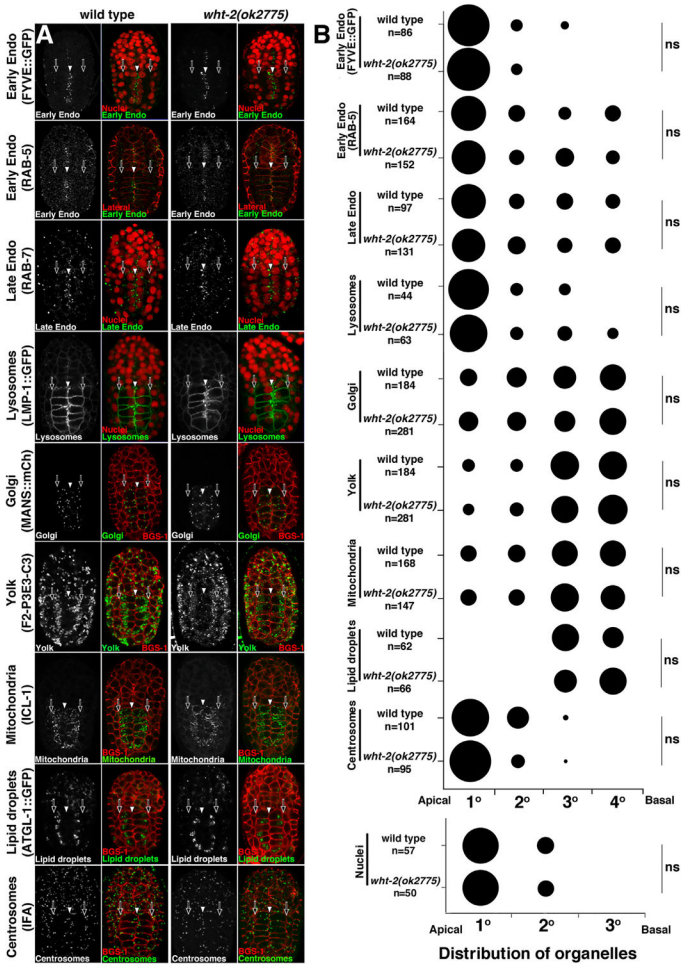

Figure 5. Organelle positioning during epithelial polarization in *wht-2(−)* mutants.

(A) Organelles in wild type or *wht-2(ok2775)* E16 stage embryos were marked with antibodies or fluorescent proteins. The apical and basal domain of intestinal cells was identified by labeling nuclei, the lateral domain, or the cell cortex. Single confocal optical sections are shown. The white arrowhead marks the apical domain and the black arrows denote the basal domain of the intestinal cells. (B) The position of organelles within individual intestinal cells was scored as described in the legend for Figure 1. The area of the circles represents the proportion of organelles located within each quadrant. A Fisher's exact test followed by a Bonferroni correction was used to compare the distribution of each type of organelle between the *wht-2(−)* mutant and wild type (ns represents a $p > 0.05$).

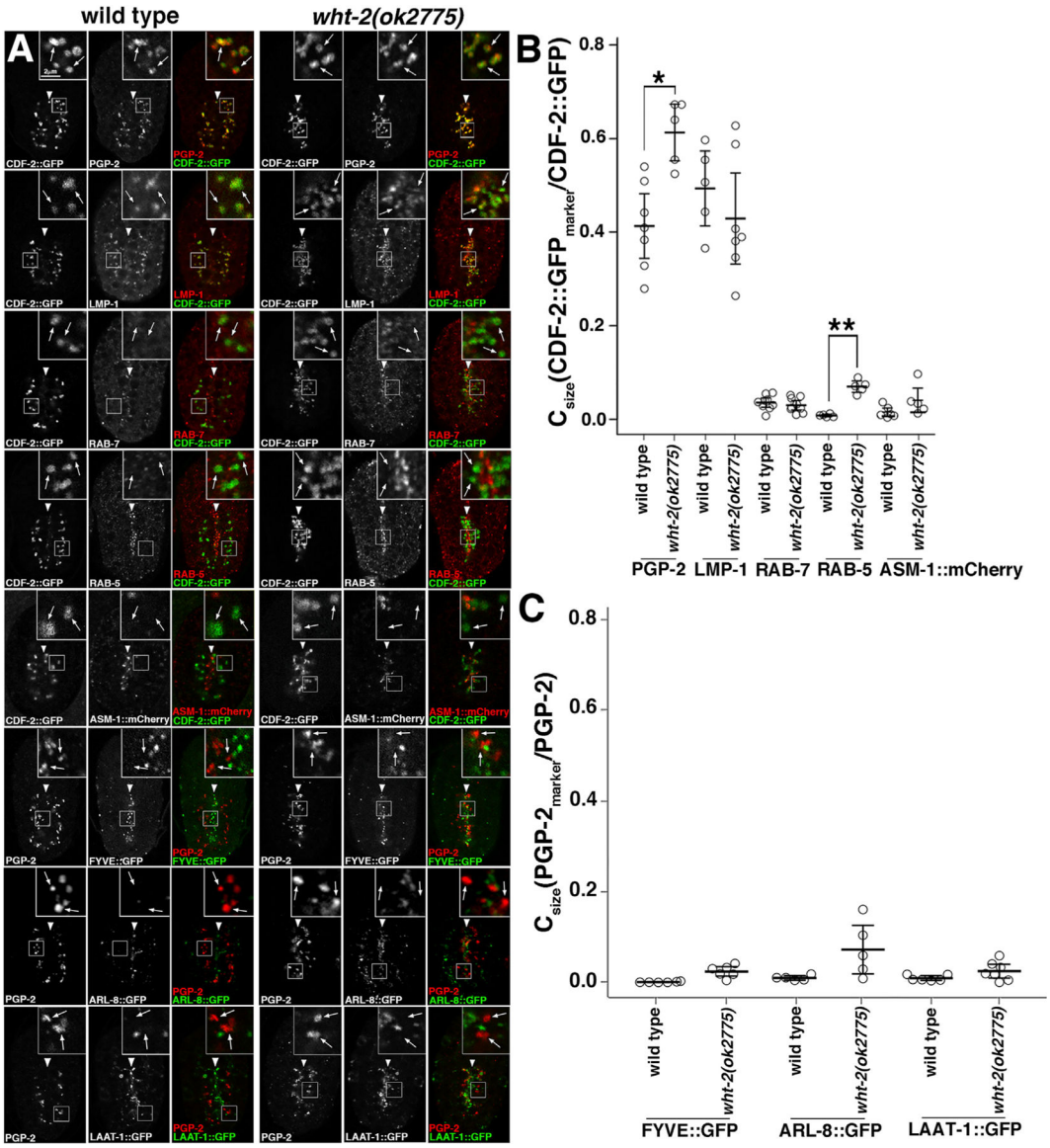

Figure 6. Gut granule identity is not altered in *wht-2(−)* mutants.

The localization of CDF-2::GFP or PGP-2 was assessed relative to gut granule or conventional endosomal markers in E16 stage embryos with confocal microscopy. In insets, white arrows denote compartments containing CDF-2::GFP or PGP-2. (B and C) SQUAASH software was used to calculate C_{size}, which describes the proportion of the total CDF-2::GFP or PGP-2 area within an embryo that also contains the indicated marker. Five to ten embryos were analyzed. The mean is plotted and the error bars represent the 95% confidence limit. Wild type and *wht-2(−)* were compared to each other with a one-way ANOVA (* represents a $p \leq 0.05$, ** represents a $p \leq 0.001$, and all others $p > 0.05$.).

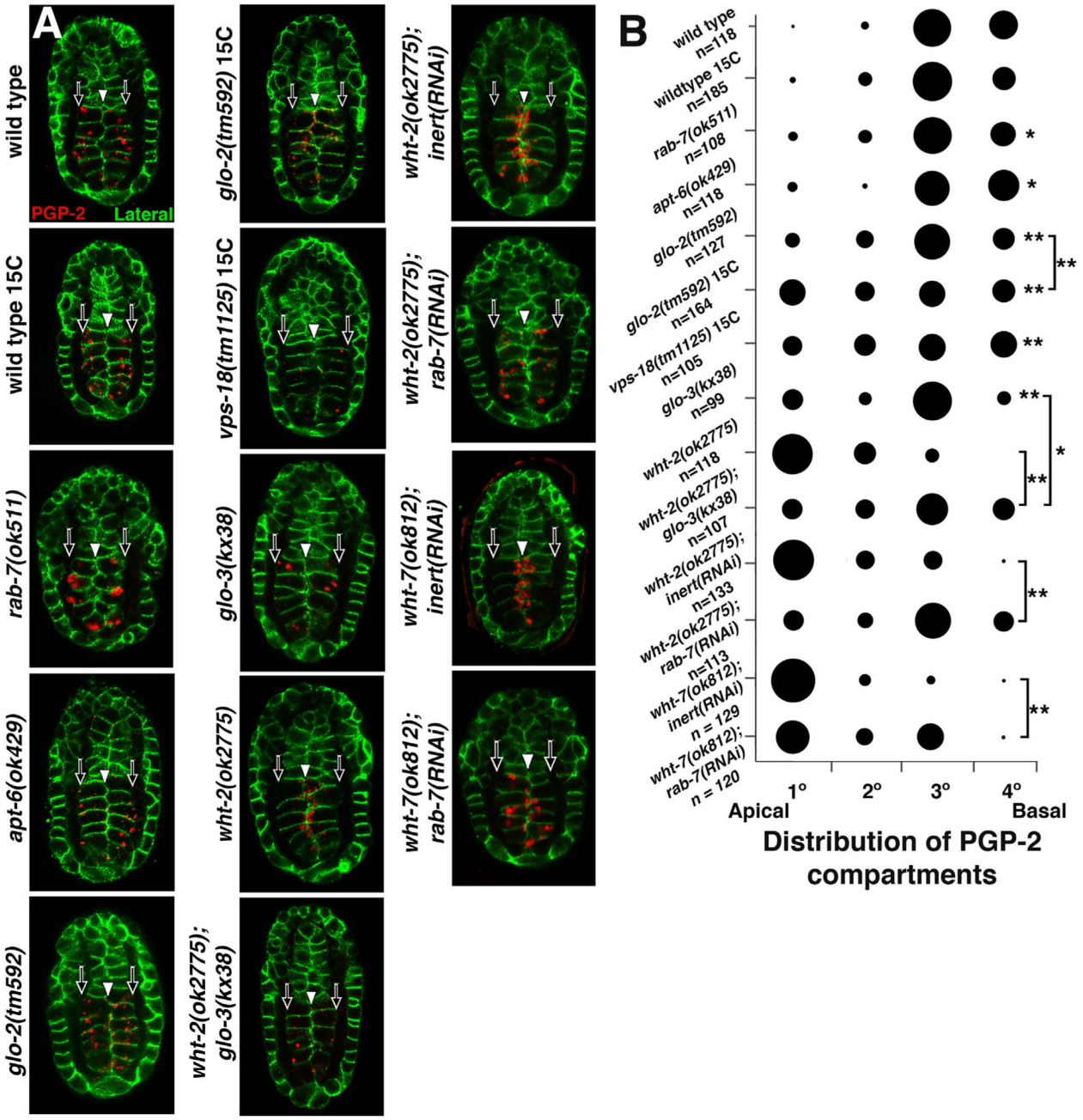

Fig 7. Gut granule biogenesis mutants disrupt the positioning of PGP-2 marked organelles during epithelial polarization.

(A) Wild-type or mutant E16 stage embryos were stained with antibodies marking PGP-2 and lateral domains and imaged with confocal microscopy. Single optical sections are shown, and white arrowheads and black arrows mark the apical and basal intestinal cell domains, respectively. Unless otherwise indicated all embryos were grown at 22C. (B) The position of organelles within individual intestinal cells was scored as described in the legend for Figure 1. The area of the circles represents the proportion of organelles located within each quadrant. A Fisher's exact test followed by a Bonferroni correction was used to

compare the distribution of PGP-2 compartment positioning in the mutants and wild type or as indicated by brackets (* represents a $p \leq 0.05$ and ** represents a $p \leq 0.001$).

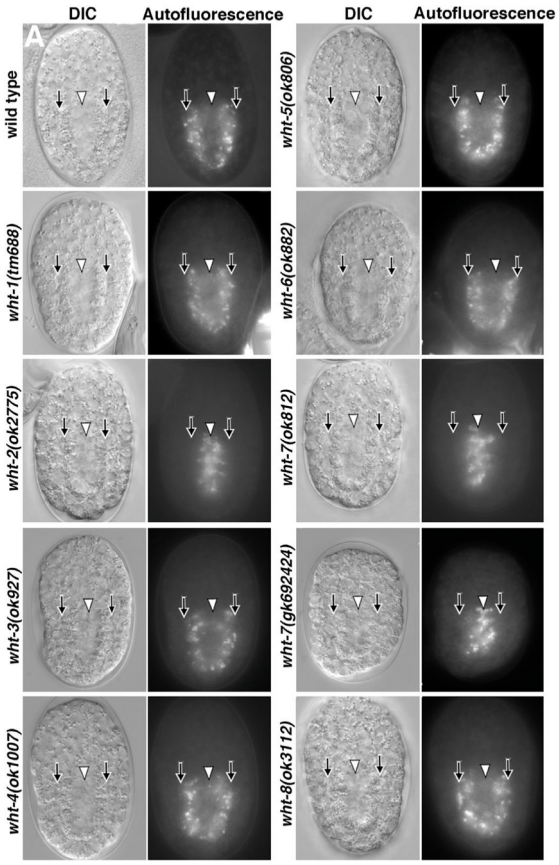

B

Genotype	Position of autofluorescent organelles apical	intermediate	basal	n
Wild type	0%	0%	100%	28
wht-1(tm688)	0%	0%	100%	27
wht-2(ok2775)	88%	0%	12%	26
*wht-2(ok2775) + wht-2(+)***	50%	0%	50%	22
wht-3(ok927)	0%	0%	100%	26
wht-4(ok1007)	0%	0%	100%	27
wht-5(ok806)	0%	0%	100%	28
wht-6(ok882)	0%	0%	100%	29
wht-7(ok812)	82%	7%	11%	28
*wht-7(ok812) + wht-7(+)***	52%	0%	48%	32
wht-7(gk692424)	82%	11%	7%	27
wht-8(ok3112)	0%	8%	92%	26

Figure 8. Screen of WHT family ABCG family proteins for gut granule positioning defects.

(A) E16 stage embryos were imaged with DIC and a DAPI fluorescence filter using wide field microscopy to identify the intestinal primordium and autofluorescent gut granules, respectively. The basal surfaces of intestinal cells are marked with black arrows and the apical surfaces are marked with white arrowheads. The DIC and DAPI images show the same optical section. (B) The pattern of gut granule positioning was quantified by categorizing the overall distribution of autofluorescent organelles within the intestinal primordium. The progeny of adults with a PCR product containing *wht-2(+)* or a fosmid containing *wht-7(+)* were scored. Extra-chromosomal arrays are lost during both meiotic and mitotic divisions so that many of the embryos scored lacked the PCR product or fosmid. A Fisher's exact test was used to compare *wht* mutant populations with the extrachromosomal array to the *wht* mutant alone (** represents $p \leq 0.005$).

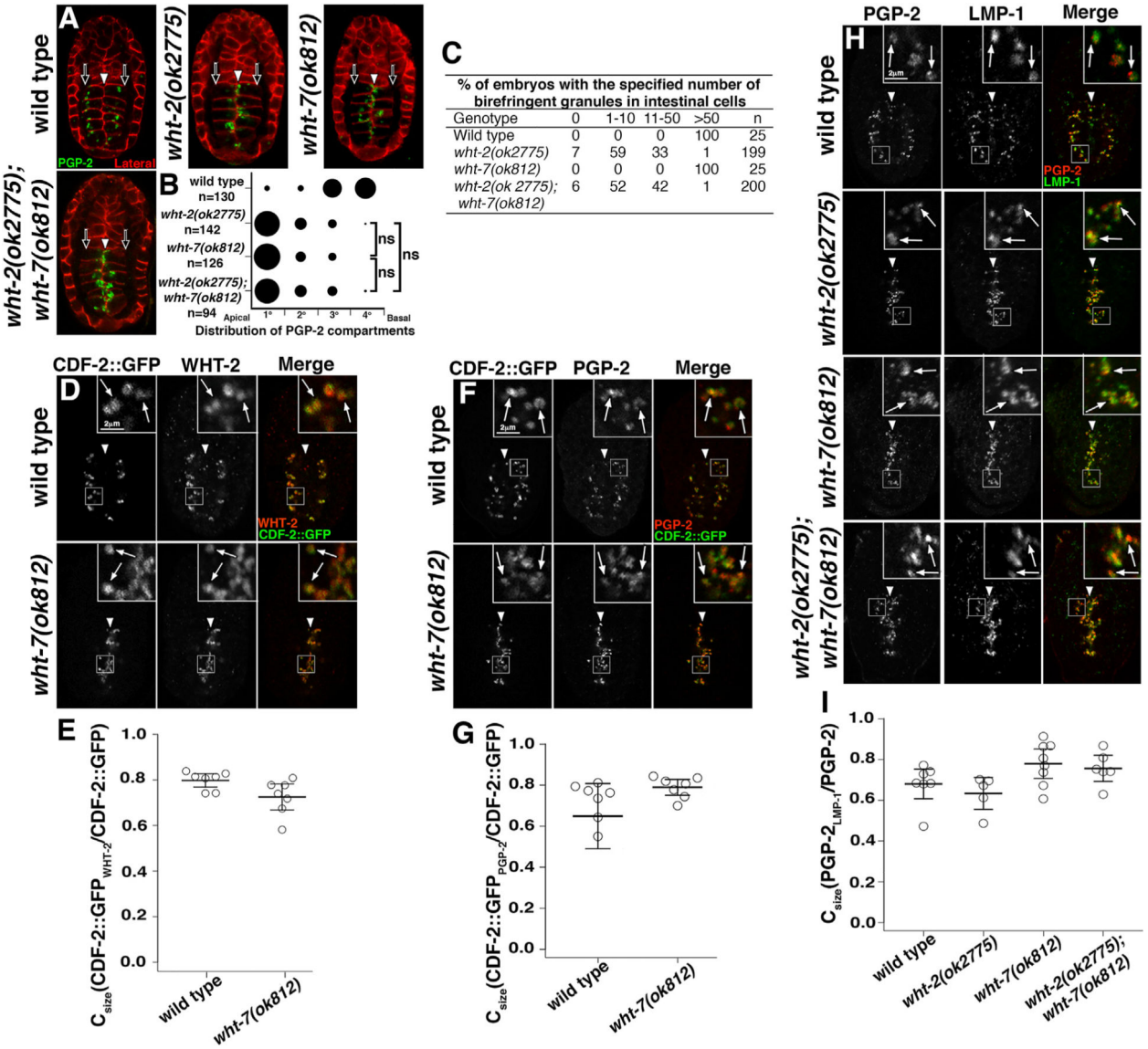

Figure 9. Effects of *wht-7(−)* on gut granule positioning and gut granule formation.

(A) E16 stage embryos were stained with antibodies marking PGP-2 and lateral domains and imaged with confocal microscopy. Single optical sections are shown, and white arrowheads and black arrows mark the apical and basal intestinal cell domains, respectively. (B) The position of organelles within individual intestinal cells was scored as described in the legend for Figure 1. The size of the circles represents the proportion of organelles located within each quadrant. A Fisher's exact test was used to compare the distribution of PGP-2 marked organelles between the single and double mutants as indicated by the brackets (ns represents a $p > 0.05$). (C) Three-fold and later stage embryos were analyzed using polarization microscopy and scored for the number of birefringent granules in the intestine. The *wht-2;wht-7* double mutant was not significantly different than *wht-2 (ok2775)* ($p > 0.05$, Fisher's exact test). (D, F, H) The relative localization of gut granule proteins CDF-2::GFP, WHT-2, PGP-2, and LMP-1 was assessed in E16 stage embryos with confocal microscopy. In insets, white arrows denote compartments containing both markers. (E, G,

I) SQUAASH software was used to calculate C_{size}, which describes the proportion of the total CDF-2::GFP or PGP-2 area within an embryo that also contains the indicated marker. Five to seven embryos were analyzed. The mean is plotted and the error bars represent the 95% confidence limit. Wild type and mutants were compared to each other with a one-way ANOVA and $p > 0.05$.

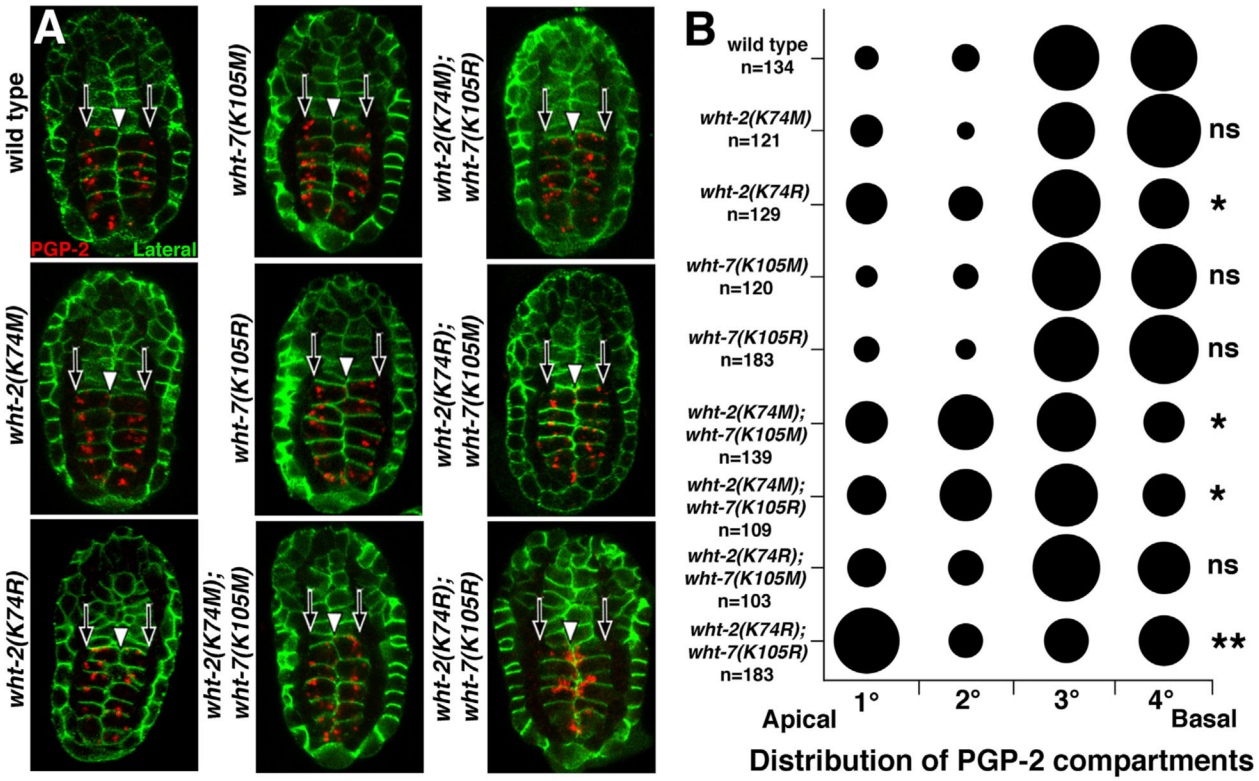

Figure 10. Gut granule positioning in WHT-2 and WHT-7 ATPase mutants.

(A) E16 stage embryos were stained with antibodies marking PGP-2 and lateral domains and imaged with confocal microscopy. Single optical sections are shown, and white arrowheads and black arrows mark the apical and basal intestinal cell domains, respectively. (B) The position of organelles within individual intestinal cells was scored as described in the legend for Figure 1. The size of the circles represents the proportion of organelles located within each quadrant. A Fisher's exact test followed by a Bonferroni correction was used to compare the distribution of PGP-2 compartment positioning in the single mutants and wild type or the double mutants and the single mutants used to construct it (ns is $p>0.05$, * is $p\leq0.05$, ** is $p\leq0.001$).

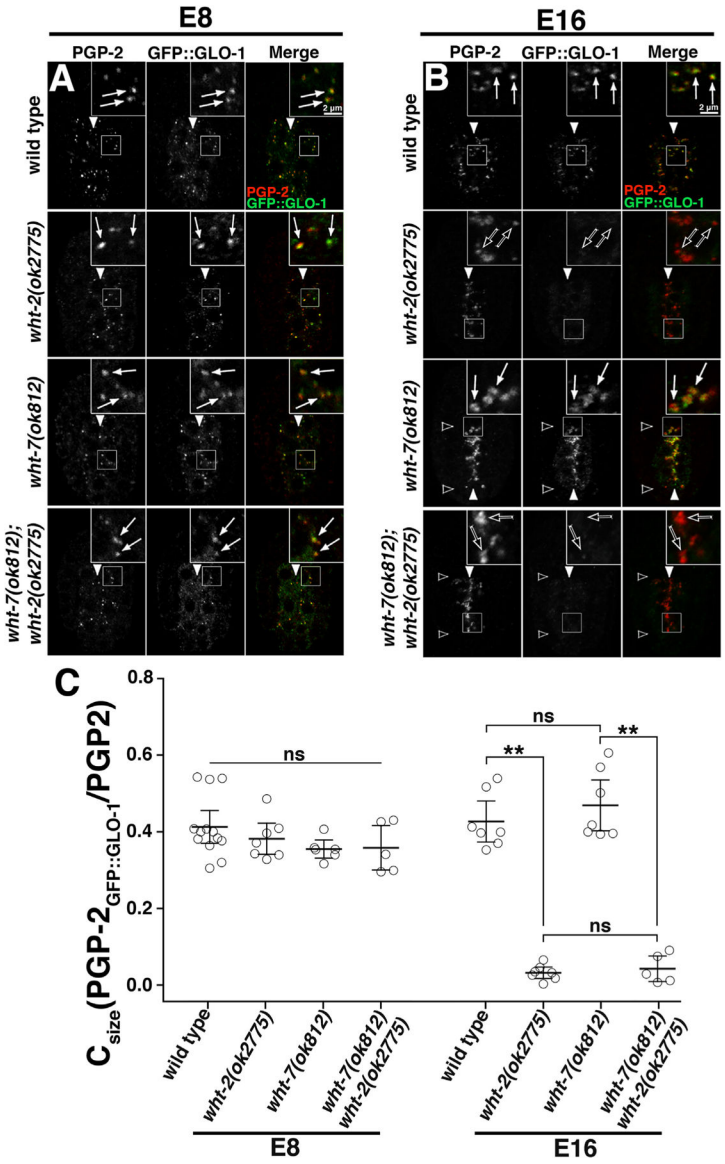

Figure 11. Effects of *wht-2(−)* and *wht-7(−)* on GFP::GLO-1 localization in E8 and E16 stage embryos.

(A) E16 stage embryos expressing GFP::GLO-1 were stained with antibodies to PGP-2 and GFP and imaged with confocal microscopy. White arrows indicate examples of GFP::GLO-1 localizing to PGP-2 compartments and black arrows indicate examples where GFP::GLO-1 is lacking from PGP-2 compartments. (B) The proportion of the total PGP-2 signal area in each embryo that also contains GFP::GLO-1 is plotted. Five to 13 embryos of each genotype were analyzed. The mean is shown and the bars represent the 95% confidence interval. Strains were compared to each other by one-way ANOVA (ns is $p>0.05$ and ** is $p\leq0.001$).

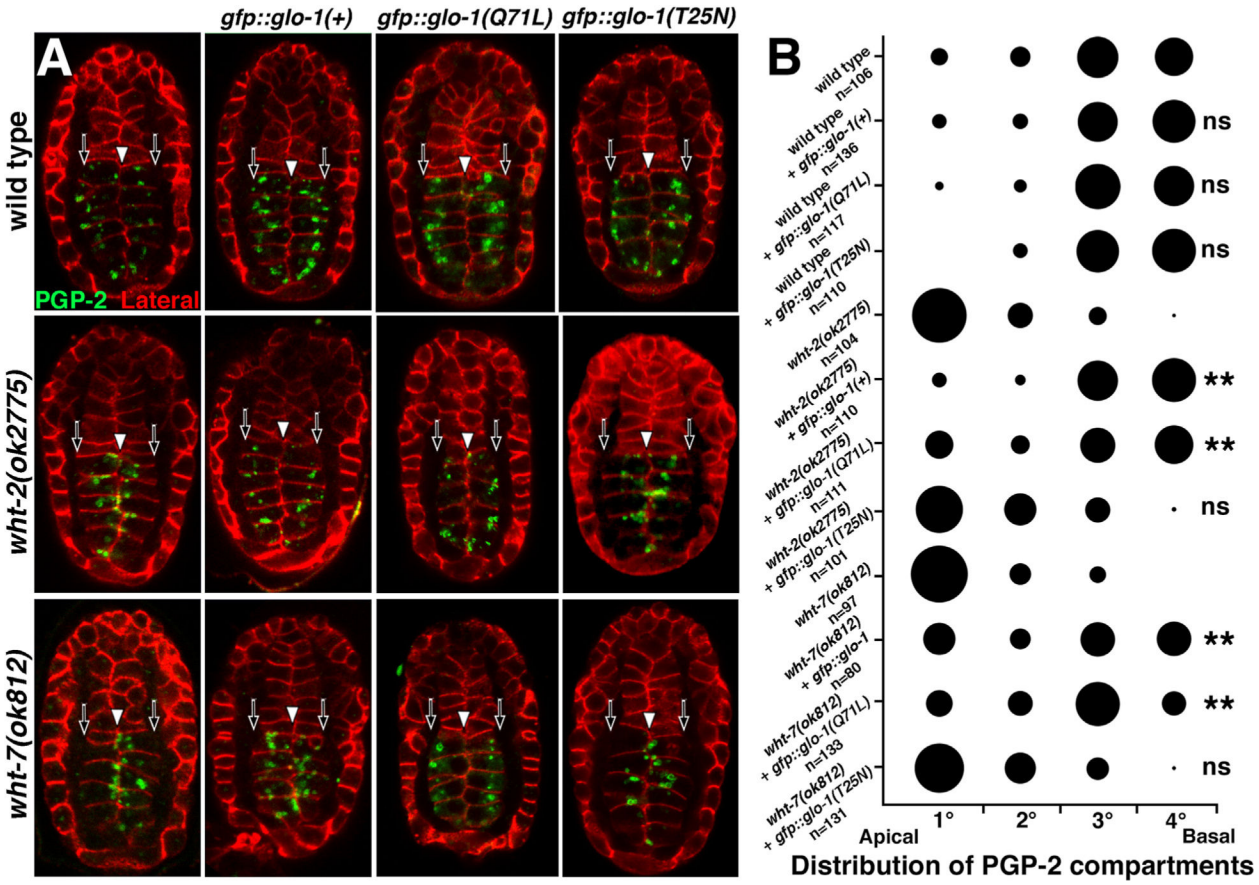

Figure 12. Expression of GLO-1 restores basal gut granule positioning in *wht-2(−)* and *wht-7(−)* mutants.

(A) E16 stage embryos lacking or expressing different forms of GFP::GLO-1 were stained with antibodies marking PGP-2 and lateral domains and imaged with confocal microscopy. Single optical sections are shown, and white arrowheads and black arrows mark the apical and basal intestinal cell domains, respectively. (B) The position of organelles within individual intestinal cells was scored as described in the legend for Figure 1. The size of the circles represents the proportion of organelles located within each quadrant. A Fisher's exact test followed by a Bonferroni correction was used to compare the distribution of PGP-2 compartment positioning in embryos expressing *gfp::glo-1* to those lacking its expression (ns is $p>0.05$ and ** is $p\leq0.001$).

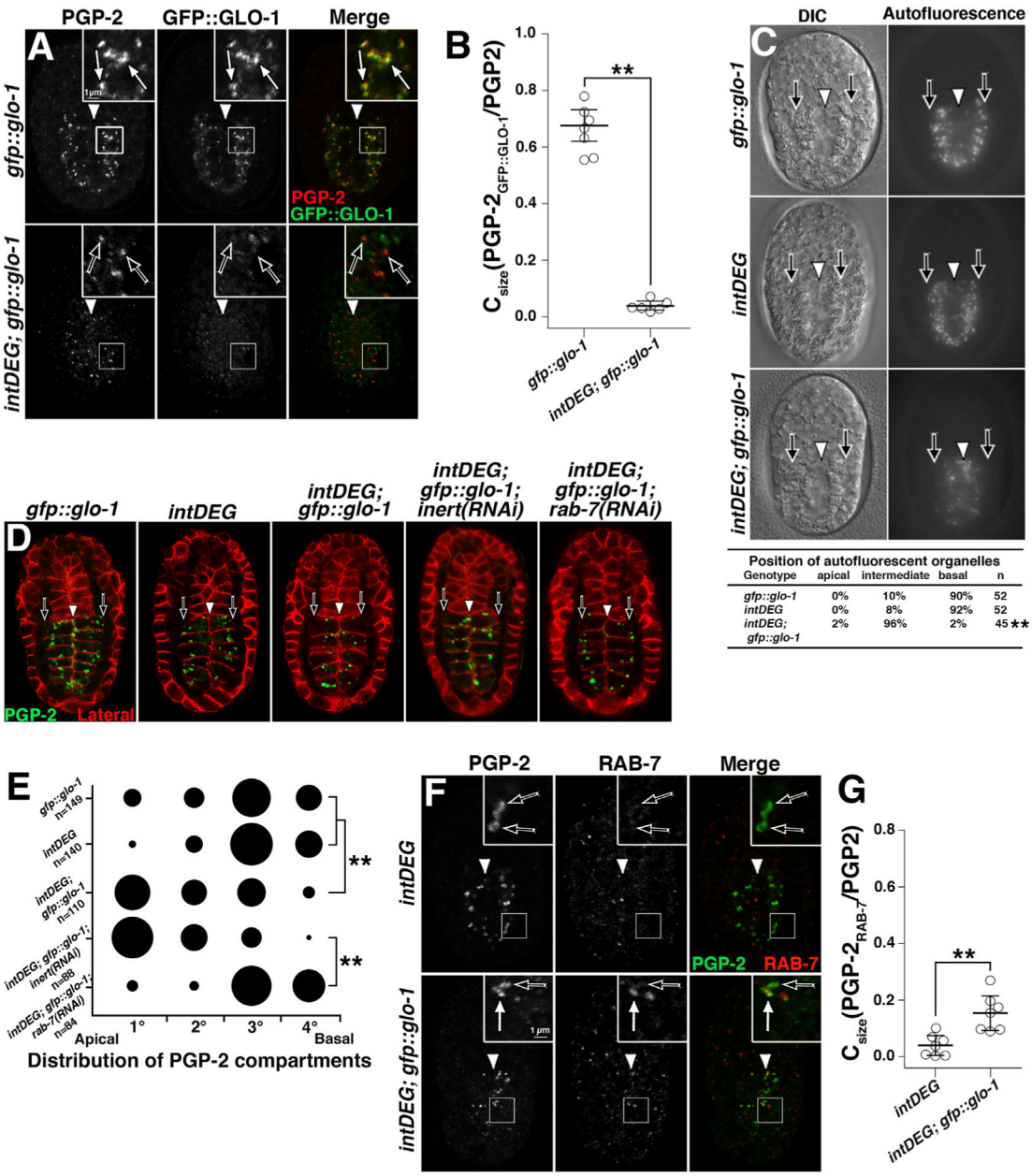

Figure 13. Role of GLO-1 in gut granule positioning during epithelial polarization.

(A) E16 stage embryos expressing *gfp::glo-1* were stained with antibodies to PGP-2 and GFP and imaged with confocal microscopy. White arrows indicate examples of GFP::GLO-1 localizing to PGP-2 compartments and black arrows indicate examples where GFP::GLO-1 is lacking from PGP-2 compartments. (B) The proportion of the total PGP-2 signal area in each embryo that also contained GFP::GLO-1 is plotted. The mean is shown and the bars represent the 95% confidence interval. Strains were compared to each other by one-way ANOVA (** is p≤0.001). (C) E16 stage embryos were imaged with DIC and a DAPI fluorescence filter using wide field microscopy and the overall distribution of autofluorescent organelles within the intestinal primordium was categorizing. The basal surfaces of intestinal cells are marked with black arrows and the apical surfaces

are marked with white arrowheads. The DIC and DAPI images show the same optical section. A Fisher's exact test was used to compare *intDEG; gfp::glo-1* with the *intDEG* and *gfp::glo-1* populations (** represents p≤ 0.005). (D) E16 stage embryos were stained with antibodies marking PGP-2 and lateral domains and imaged with confocal microscopy. Single optical sections are shown, and white arrowheads and black arrows mark the apical and basal intestinal cell domains, respectively. (E) The position of organelles within individual intestinal cells was scored as described in the legend for Figure 1. In E, the size of the circles represents the proportion of organelles located within each quadrant. A Fisher's exact test was used to compare the distribution of PGP-2 compartment positioning in the indicated strains (** is p≤0.001). (F) E16 stage embryos were stained with antibodies to PGP-2 and RAB-7 and imaged with confocal microscopy. White arrows indicate examples of RAB-7 localizing to PGP-2 compartments and black arrows indicate examples where GFP::GLO-1 is lacking from PGP-2 compartments. (G) The proportion of the total PGP-2 signal area in each embryo that also contained RAB-7 is plotted. The mean is shown and the bars represent the 95% confidence interval. Strains were compared to each other by one-way ANOVA (** is p≤0.001).